Transportation Research Part C 95 (2018) 748–772

Contents lists available at ScienceDirect

Transportation Research Part C

journal homepage: www.elsevier.com/locate/trc

Dynamic charging infrastructure deployment for plug-in hybrid electric trucks

Zhaocai Liu, Ziqi Song*

Department of Civil and Environmental Engineering, Utah State University, Logan, UT 84322-4110, United States

ARTICLE INFO

Keywords:
Plug-in hybrid electric trucks
Electrified road freight transportation
Dynamic charging lane
Equilibrium
Deployment plan
Robust optimization

ABSTRACT

Inspired by the rapid development of charging-while-driving (CWD) technology, plans are ongoing in government agencies worldwide for the development of electrified road freight transportation systems through the deployment of dynamic charging lanes. This en route method for the charging of plug-in hybrid electric trucks is expected to supplement the more conventional charging technique, thus enabling significant reduction in fossil fuel consumption and pollutant emission from road freight transportation. In this study, we investigated the optimal deployment of dynamic charging lanes for plug-in hybrid electric trucks. First, we developed a multi-class multi-criteria user equilibrium model of the route choice behaviors of truck and passenger car drivers and the resultant equilibrium flow distributions. Considering that the developed user equilibrium model may have non-unique flow distributions, a robust deployment of dynamic charging lanes that optimizes the system performance under the worst-case flow distributions was targeted. The problem was formulated as a generalized semi-infinite min-max program, and a heuristic algorithm for solving it was proposed. This paper includes numerical examples that were used to demonstrate the application of the developed models and solution algorithms.

1. Introduction

Trucks are an important part of modern freight transportation. According to the American Trucking Association (ATA) (2016a), trucks were used for the transportation of 70.1% of the domestic freight tonnage in the United States in 2015, accounting for 81.5% of the nation's total freight bill. With the growth of the national economy, particularly in manufacturing, consumer spending, and international trade, it is forecasted that the truck tonnage will increase by 27% between 2016 and 2027 (ATA, 2016b). However, current trucks are mainly powered by fossil fuel, which have a low energy efficiency and high level of exhaust emission. A recent study by the American Transportation Research Institute (ATRI) found that more than 99.5% of trucks in the United States in 2016 utilized fossil fuel (Torrey and Murray, 2016). Moreover, most medium and heavy trucks use diesel fuel, which accounts for 89.6% of the energy consumption by medium and heavy trucks in the United States in 2014 (Davis et al., 2016). Diesel engines are a primary source of particulate matter (PM) and nitrogen oxides (NOx) emissions, and the development of a more sustainable road freight transportation system requires the urgent replacement of diesel-engine trucks with more energy-efficient and low-emission trucks.

Among the available alternative powertrains for trucks, plug-in hybrid electric truck (PHET) technology is widely considered to be promising for achieving significant increase in fuel economy and decrease in emission (e.g., Burton et al., 2013; CalETC, 2015; Johannesson et al., 2015; Okui, 2016). Compared to conventional internal combustion engine (ICE) trucks, the advantages of PHETs are twofold. First, when fully charged, the on-board battery pack of a PHET is capable of substituting a significant amount of fossil

* Corresponding author.
E-mail address: ziqi.song@usu.edu (Z. Song).

https://doi.org/10.1016/j.trc.2018.08.011
Received 27 March 2018; Received in revised form 9 August 2018; Accepted 23 August 2018
Available online 06 September 2018
0968-090X/

fuel consumption. Second, the combination of an ICE and electric motor improves the energy efficiency through the optimization of the engine operation and recovery of kinetic energy during braking. Furthermore, battery electric truck (BET) technologies are not currently mature enough for long-haul operations. Sripad and Viswanathan (2017) estimated that the battery pack of a 600-mile BET would weigh over 18 tons while its available payload is capped at 12 tons, implying that a BET would consume a greater fraction of energy in moving its battery pack rather than its payload. On the other hand, a PHET avoids the disadvantages of the limited driving range and long charging time of BETs. As reported in CalETC (2015), freight operators typically use a given truck for multiple routes of varying distances, and a PHET affords flexibility in daily operation, enabling greater utilization.

Although PHETs enable significant reduction of fossil fuel consumption relative to their diesel- and gasoline-engine counterparts, owing to battery technology limitations, long-distance road freight transportation using the electric-only mode is currently uneconomical and impractical. However, recent breakthroughs in charging technologies promise to enhance the utilization of PHETs. Among these innovative technologies, charging-while-driving (CWD) (Deflorio and Castello, 2017; Chen et al., 2018) has great potential for the future. Segments of existing roads can be converted into dynamic charging lanes through the installation of conductive or inductive charging facilities. PHETs equipped with the appropriate power receivers can then charge their batteries while traveling on such roads. This would enable further reduction of fossil fuel consumption by PHETs. In addition, PHETs enable drivers to operate them as conventional trucks outside dynamic charging lanes. In the light of the forgoing, the present study focused on the deployment of dynamic charging infrastructure for PHETs used for long-haul road freight transportation.

Conductive-charging-based CWD has been applied in electric trains and trams for more than a century. Siemens adapted the technology for trucks and developed the so-called eHighway system that can electrify road freight transportation (Grünjes and Birkner, 2012). The application of inductive charging to electric vehicles was also proposed as early as 1990s by California's Partner for Advanced Transit and Highways (PATH) (PATH, 1996). Since then, numerous studies have been conducted to improve and verify the feasibility of the innovation (e.g., Covic et al., 2000; Boys et al., 2002; Huang et al., 2009; Huh et al., 2011; Choi et al., 2013; Cirimele et al., 2014; Chen et al., 2015; Fuller, 2016). The Korea Advanced Institute of Science and Technology (KAIST) in South Korea developed an online electric vehicle (OLEV) system that utilizes dynamic wireless charging technology, and implemented it in the KAIST campus shuttle system (Suh et al., 2011). Utah State University constructed an electrified test track and demonstrated that in-motion electric vehicles could be effectively and safely charged through dynamic wireless charging (Morris, 2015; Limb et al., 2016; Liu and Song, 2017; Liu et al., 2017). As argued by Chen et al. (2017), commercial fleets, such as bus and truck fleets, are likely to be the early users of dynamic charging infrastructure because of the higher benefits that they stand to gain. The commercialization of CWD technology is indeed on the horizon. The OLEV system has already been applied to the trolley system at the Seoul Grand Park and a bus line in Gumi City (Jang et al., 2015). Scania and Siemens have also built a two-kilometer electric road on the E16 motorway in Sweden (Scania, 2016). Further, Siemens has worked with the South Coast Air Quality Management District (SCAQMD) in California to install and demonstrate the eHighway system in the proximity of the ports of Los Angeles and Long Beach (Siemens, 2015).

The effective utilization of CWD technology for road freight transportation requires the strategic deployment of the charging lanes in parts of the road network connecting logistics centers, such as ports, terminals, and distribution centers. This paper proposes a network modeling framework for improving the system performance by optimizing the locations of the charging lanes under limited budget.

To determine the optimal strategy for deploying charging lanes in a transportation network, a user equilibrium (UE) model should first be developed to describe the effect of a new design plan on the route choice behaviors of drivers, and the resulting traffic flow distributions. This study considered mixed traffic of passenger cars and trucks. We further envision that, to develop a sustainable road freight transportation system, the government and freight companies would work together to convert freight trucks using the network into PHETs, and deploy charging lanes for the trucks. The route choice behaviors of PHET drivers in a network with charging lanes should be explicitly considered in the UE model. There have been a few previous studies on the formulation of a network equilibrium model for electric vehicles. Considering the limited travel range of battery electric vehicles (BEVs), Jiang et al. (2012) introduced a path constraint for restricting the length of the paths usable by electric vehicles into a conventional UE model. Jiang et al. (2014) and Jiang and Xie (2014) investigated the network equilibrium problems involving mixed gasoline and electric vehicle flows. He et al. (2014, 2015, 2016), Xie and Jiang (2016) and Zheng et al. (2017) further developed a series of UE models in which the range of BEVs could be extended by charging at public charging stations. Wang et al. (2016) incorporated trip chain analysis into the UE problem involving BEVs. Xie et al. (2017) further extended this study by considering stochastic range anxiety of BEV users. Considering battery swapping and road grade, Xu et al. (2017) investigated network UE problems with mixed BEVs and gasoline vehicles. Nevertheless, charging lanes have not been considered in these studies. Chen et al. (2016) considered a futuristic road network with charging lanes and used by only BEVs, and built a novel user equilibrium model using modified equilibrium conditions. In their study, BEVs have limited battery capacity and may need to be recharged on charging lanes to ensure they have enough energy to reach their destinations. BEV users are assumed to select routes to minimize their travel time cost while ensuring not to run out of charge before reaching their destinations. In contrast, PHET drivers considered in our study do not have range anxiety and can have quite different route choice behaviors compared to BEV drivers.

The route choice behaviors of PHET drivers could be influenced by charging lanes. In conventional UE traffic assignment studies (e.g. Sheffi, 1985), travel time is often used as the sole criterion for route choices for travelers. Fuel cost can be neglected because it is highly correlated with travel time and thus exhibits the same trend with travel time. However, for PHETs in a transportation network with charging lanes, fuel cost and travel time could have quite different trends. Due to the fact that electric motors are much more efficient than ICEs, using electricity as vehicle fuel can reduce fuel cost by approximately 50% compared to using fossil fuel (Alternative Fuels Data Center, 2017). Therefore, for PHETs, a route with high travel time could have low fuel cost if charging lanes are deployed along the route to electrify the driving mode of these PHETs. Because PHET drivers can significantly reduce their fuel

cost through consuming electricity instead of fossil fuel, they will prefer electric-powered driving mode and routes with charging lanes. In this study, we consider that PHET drivers will attempt to minimize their generalized total travel cost when choosing routes, which is a combination of travel time and fuel cost. When traveling from their origins to destinations, PHET drivers can select their routes, driving modes, and charging plans. To minimize their total travel cost, PHET drivers need to determine the best trade-off between travel time and fuel cost. In this study, the route choice behavior of PHET drivers in a transportation network with charging lanes was explicitly modeled. A multi-class multi-criteria UE (MMUE) model was then formulated to describe the traffic flow distribution in the road network.

Based on the proposed UE model, we then explored the optimal deployment strategy for charging lanes in a general network. Only a limited number of studies have investigated the deployment problem of charging lanes. Riemann et al. (2015) proposed a flow-capturing location model to optimize the deployment of charging lanes in a network. Fuller (2016) presented a flow-based set covering model to minimize the total capital cost of deploying charging lanes in California. Chen et al., (2016) formulated a bi-level deployment model considering UE conditions to optimize the locations of charging lanes with limited budget. Chen et al. (2017) investigated the deployment of stationary charging stations and dynamic charging lanes along long traffic corridors under both public and private provision. In this study, we consider the charging lane deployment problem as a generalized bi-level network design problem (NDP), in which the upper-level problem determines the optimal location for deploying charging lanes and the lower-level problem accounts for the route choice behavior of passenger car and truck drivers. NDP has been extensively studied in transportation planning (e.g., Wang et al., 2015; Farvaresh and Sepehri, 2011; Yamada and Febri, 2015; Song et al., 2017; He et al., 2018). For an overview on NDP, refer to, for instance, Boyce (1984), Friesz (1985), Bell and Iida (1997), Yang and Bell (1998), Farahani et al. (2013). In bi-level NDP, the objective of the upper-level problem is to optimize a predetermined system performance measure. Because charging lanes can significantly reduce fossil fuel consumption by PHETs and thus will also help to reduce tailpipe emissions and promote environmental sustainability of road freight transportation, fuel consumption and vehicle emissions can be reasonable parts of the system performance measure for a network with charging lanes. Moreover, charging lanes also influence network users' route choice behaviors and travel time cost. Therefore, we consider the sum of system travel time cost, fuel cost, and emission cost as the system performance measure. The charging lane deployment problem can further be classified as the bi-level transportation problem with environmental considerations. Considering environmental sustainability in transportation network design is essential for sustainable transportation development and has been investigated in the literature (Szeto et al., 2012; Xu et al., 2016).

In conventional NDPs, the UE model for the lower-level problem usually has a unique flow distribution and origin-destination (O-D) equilibrium travel cost, thus a new design or plan can be easily evaluated based on the resulting equilibrium solution. However, UE model proposed in this study may have non-unique solutions for link flow distributions and O-D travel cost. With non-unique UE solutions, the corresponding system performance may also be non-unique. Therefore, new assessment principle needs to be proposed to evaluate the system performance of a design under non-unique UE solutions. In practice, a design that can perform well even in the worst-case scenario is more robust and preferable for planners who tend to be risk-averse. Following the notion of robust optimization (e.g., Ben-Tal and Nemirovski, 2002), we proposed a model of deploying charging lanes to optimize the system performance under the worst-case UE flow distribution.

The contributions of this paper are multidimensional. First, we make the first attempt to utilize a bi-level network modeling framework to investigate the application of dynamic charging lanes and PHETs in reducing fossil fuel and exhaust emissions from road freight transportation. Second, we develop a multi-class multi-criteria user equilibrium (MMUE) model to describe the traffic flow distribution in a transportation network with charging lanes and mixed traffic of passenger cars and trucks. The proposed model can capture the specific route choice and driving behaviors of PHET users. Third, based on the proposed MMUE model, we investigated the optimal deployment strategy for charging lanes in a general network. We identified that, the MMUE problem may have non-unique solutions for link flow distributions and O-D travel cost and thus the system performance of a deployment plan may also be non-unique. Considering this non-uniqueness property, we proposed a robust optimization model to determine the deployment of charging lanes.

The remainder of this paper is organized as follows. Section 2 presents the basic considerations and assumptions of the present study. Section 3 describes the development of the proposed MMUE model and discusses its property and solution algorithm. The problems of determining the respective system performance for the best-case and worst-case scenarios based on the non-unique equilibrium flow patterns are also formulated as mathematical programs with complementarity constraints (MPCCs). Section 4 describes the development of the robust optimization model for determining the optimal deployment of charging lanes, and presents the heuristic algorithm for solving it. Section 5 uses a few numerical examples to demonstrate the use of the proposed model. Finally, Section 6 concludes the paper.

2. Basic considerations

In this study, we considered a transportation network connecting logistics centers, which is thus significantly used by trucks. To develop a sustainable road freight transportation system, we assumed that the government and freight companies would work together to convert freight trucks using the network into PHETs (e.g., through retrofitting their engines), and deploy charging lanes for the trucks. As noted earlier, when traveling between their origin and destination, PHET drivers make effort to minimize the total travel cost, which is determined by the travel time and fuel cost. They choose their route, decide on whether to use electric energy, and whether and for how long to recharge their batteries on the charging lanes. Before the state of charge (SOC) of the on-board battery of a PHET reaches zero or a predefined lower limit, the driver can always choose to use electricity instead of fossil fuel to reduce fuel cost. Moreover, when traveling on a charging lane, the potential charging time of a PHET is determined by its speed,

which is thus another critical decision for PHET drivers.

The primary objective of this study was to strategically determine the optimal deployment of charging lanes for PHETs. The development of the utilized model was based on the following basic assumptions:

I. A link in the network is either an ordinary or charging link. All the lanes of a charging link are charging lanes. This assumption is not restrictive because charging lanes can always be represented by separate links.
II. The network is used by mixed traffic of both freight trucks and passenger cars. When choosing their routes, drivers attempt to minimize the total travel cost. For PHETs, the travel cost is determined by the travel time and fuel cost. For other vehicles, the travel time is the only concern. In conventional traffic assignment studies (e.g., Sheffi, 1985), the fuel cost was usually neglected because it is highly correlated with travel time and thus exhibits the same trend with travel time. However, PHETs can significantly save fuel cost through getting recharged on charging lanes and using electric energy instead of fossil fuel (Gao et al., 2017).
III. A PHET driver can decide whether to charge his or her vehicle when traveling on a charging lane. The charging time is thus less than or equal to the travel time on the charging lane. The amount of electric energy charged is the product of the charging time and a predetermined constant charging rate.
IV. When on a charging lane, a PHET driver can decide the travel time by adjusting their travel speed. The maximum travel speed is determined by the link performance function based on the traffic flow on the link (Yang et al., 2015; Chen et al., 2016), while the minimum travel speed is a predetermined lower speed limit, which is less than or equal to the maximum allowable speed. This assumption is to accommodate the situation in which drivers may want to obtain more energy from the dynamic charging infrastructure by intentionally slowing down.
V. The travel time of a vehicle that is not PHET on a link is determined by the traffic flow on the link, which can be specified by the link performance function and is not affected by the speeds of PHET drivers. It is always possible for a fast-moving vehicle to perform an overtaking maneuver when it catches up with a slow-moving vehicle (Chen et al., 2016).
VI. For a PHET, the respective tank-to-wheel efficiencies in the electric and diesel-fueled modes and the fuel consumption on a link are all predetermined constants. In previous studies involving electric vehicles (e.g., Jiang et al., 2012; Jiang and Xie, 2014; He et al., 2015, 2016; Chen et al., 2016), the electricity consumption on a link was also assumed to be constant. Moreover, in Jiang and Xie (2014) and Jiang et al. (2014), it is assumed that vehicle operating costs of both gasoline vehicles and BEVs, which are mainly fuel costs, are proportional to driving distance. In reality, however, fuel consumption may be related to travel time as well as vehicle acceleration and deceleration. Therefore, it may be more accurate to consider flow-dependent or speed-dependent fuel efficiency and fuel consumption models. However, doing so appears to be mathematically intractable, we leave it for our future studies.

3. Multi-class multi-criteria network equilibrium model

3.1. Network representation

Let $G(N, A)$ denote a road network, where N is the set of nodes and A is the set of directed links. Further, let $\hat{L}$ denote the set of candidate charging links, and L the set of links that are not considered for the deployment of charging lanes. $\hat{L}$ and L are two mutually exclusive sets and satisfy $\hat{L} \cup L = A$. Each link in the road network is denoted by $a \in A$, or a pair of nodes (i, j), where $i, j \in N$. Let M denote the set of user classes in the road network. Each user class has uniform value of time and uses the same type of vehicles with identical size, weight and fuel efficiency. As noted previously, mixed traffic of freight trucks and passenger cars were considered in this study. To differentiate PHET users from other users, let $M1 \subset M$ denote the set of all classes of PHET users and $M2 = M \backslash M1$ represent other user classes. Let W be the set of origin-destination (O-D) pairs. We use q_m^w and R_m^w to represent the travel demand and set of routes for O-D pair $w \in W$ and class $m \in M$. Further, let f_r^m denote the traffic flow of class $m \in M$ on path $r \in R_m^w$; and for an O-D pair $w \in W$, let $O(w)$ and $D(w)$ denote the origin and destination nodes, respectively. A binary variable y_a is introduced to indicate whether to deploy charging lanes on a candidate link $a \in \hat{L}$. $y_a = 1$ implies that the candidate link should be converted into a charging link; otherwise, $y_a = 0$. A detailed notation list is presented in Appendix A.

3.2. Total link flow in passenger car equivalence (PCE)

If h_a^m denotes the total link flow of vehicle class $m \in M$ on link $a \in A$, then

$$h_a^m = \sum_{w \in W} \sum_{r \in R_m^w} f_r^m \delta_a^r \quad \forall\, a \in A,\, m \in M$$

where δ_a^r is the route-link incidence. $\delta_a^r = 1$ if link $a \in A$ is on route $r \in R_m^w$; otherwise, $\delta_a^r = 0$.

If v_a denotes the total link flow in the PCE, including the flows of trucks and passenger cars on link $a \in A$, v_a can be calculated using the following equation:

$$v_a = \sum_{m \in M} h_a^m \gamma^m \quad \forall\, a \in A$$

where γ^m is the factor used for the PCE conversion of the total link flow of class $m \in M$. A constant PCE was adopted in this study to

enable the mathematical tractability of the developed model. Liang et al. (2011, 2013) and de Andrade et al. (2017) used a variable PCE to investigate the multi-class network equilibrium problem. The incorporation of a variable PCE into the present model will be undertaken in a future study.

3.3. PHET drivers' route choice behavior

Let $t_a(v_a)$ denote the travel time on link $a \in A$ for total PCE link flow v_a; it is determined by the link performance function. For a deployed charging link $a \in \hat{L}$ and $y_a = 1$, $t_a(v_a)$ is the minimum travel time, although a PHET driver may slow down to achieve a longer travel time and obtain more energy from the charging link. If $\tau_a^{m,r}$ denotes the actual travel time that a class m PHET driver spends on a charging link a along route r, and $\hat{\tau}_a^{m,r}$ the corresponding recharging time, obviously $\hat{\tau}_a^{m,r} \le \tau_a^{m,r}$. Given the minimum speed limit for each charging link a, if $\bar{t}_a$ denotes the corresponding maximum allowable travel time, according to assumption IV in Section 2, the travel time of a PHET driver on charging link a would be between $t_a(v_a)$ and $\bar{t}_a$, i.e., $t_a(v_a) \le \tau_a^{m,r} \le \bar{t}_a$. It should be noted that, if there is no minimum speed limit, the constraint $\tau_a^{m,r} \le \bar{t}_a$ can be omitted.

On a link $a \in A$ along route r, a PHET driver may decide on whether to drive in the electric mode. Let $e_a^{m,r}$ and $d_a^{m,r}$ respectively denote the electricity and diesel consumptions of a class m PHET on a link $a \in A$ along route r. $e_a^{m,r}$ would be zero if the driver does not use electricity on the link, while $d_a^{m,r}$ would be zero if the driver opts for an all-electric mode. If ϖ_a^m denotes the predetermined total energy consumption of the PHET on a link a for class $m \in M1$, the following would hold:

$$\varpi_a^m = e_a^{m,r} TWE^m + d_a^{m,r} TWD^m$$

where TWE^m and TWD^m are respectively the given tank-to-wheel efficiency of the electric motor and diesel engine of the class m PHET.

We define $c_a^{m,r}$ as the generalized travel cost of a class m PHET on link $a \in A$ along route r. It is given by

$$c_a^{m,r} = \begin{cases} t_a(v_a) VOT^m + e_a^{m,r} VOE + d_a^{m,r} VOD, & a \in L(r) \\ [(1-y_a) t_a(v_a) + y_a \tau_a^{m,r}] VOT^m + e_a^{m,r} VOE + d_a^{m,r} VOD, & a \in \hat{L}(r) \end{cases}$$

where VOT^m is the value of time for class m users; VOE and VOD are respectively the value or price of fuel for one unit of electricity and diesel; $L(r)$ denotes the set of links that are not considered for the deployment of charging lanes along route $r \in R_m^w$; and $\hat{L}(r)$ denotes the set of candidate charging links on the same route. It should be noted that, if a candidate charging link $a \in \hat{L}(r)$ is eventually not converted into a charging link, i.e., $y_a = 0$, a PHET driver will simply treat it as a conventional link and not consider slowing down on it.

When traveling between an O-D pair, a PHET driver attempts to minimize their generalized total cost. This involves appropriate selection of the followed route, the power utilized on each link, and whether and for how long to charge on charging links. For a route $r \in R_m^w$ in a given charging link configuration and traffic flow distribution (i.e., with constant $\{\cdots, y_a, \cdots\}$ and $\{\cdots, v_a, \cdots\}$), the optimal driver decision to minimize the generalized total cost can be determined by the following mathematical program (P1), the decision variables of which include the electricity consumption, diesel consumption, actual travel time, recharging time, and battery level:

$$P1: \min_{\boldsymbol{e},\boldsymbol{d},\boldsymbol{\tau},\hat{\boldsymbol{\tau}},\boldsymbol{E}} \sum_{a \in \hat{L}(r)} (((1-y_a) t_a(v_a) + y_a \tau_a^{m,r}) VOT^m + e_a^{m,r} VOE + d_a^{m,r} VOD) + \sum_{a \in L(r)} (t_a(v_a) VOT^m + e_a^{m,r} VOE + d_a^{m,r} VOD)$$

$s.t.$

$$e_a^{m,r} TWE^m + d_a^{m,r} TWD^m = \varpi_a^m \quad \forall a \in A(r) \tag{1}$$

$$E_j^{m,r} - E_i^{m,r} + e_a^{m,r} = 0 \quad \forall (i,j) = a \in L(r) \tag{2}$$

$$E_j^{m,r} - E_i^{m,r} + e_a^{m,r} - y_a \hat{\tau}_a^{m,r} \varepsilon = 0 \quad \forall (i,j) = a \in \hat{L}(r) \tag{3}$$

$$E_{O(w)}^{m,r} = E_0^m \tag{4}$$

$$E_i^{m,r} \le E_{max}^m b_{up}^m \quad \forall i \in N(r) \tag{5}$$

$$E_i^{m,r} \ge E_{max}^m b_{lo}^m \quad \forall i \in N(r) \tag{6}$$

$$\hat{\tau}_a^{m,r} - \tau_a^{m,r} \le 0 \quad \forall a \in \hat{L}(r) \tag{7}$$

$$\tau_a^{m,r} - \bar{t}_a \le 0 \quad \forall a \in \hat{L}(r) \tag{8}$$

$$t_a(v_a) - \tau_a^{m,r} \le 0 \quad \forall a \in \hat{L}(r) \tag{9}$$

$$e_a^{m,r} TWE^m \le \varpi_a^m \quad \forall a \in A(r) \tag{10}$$

$$d_a^{m,r} TWD^m \le \varpi_a^m \quad \forall a \in A(r) \tag{11}$$

$$\hat{\tau}_a^{m,r} \ge 0 \quad \forall a \in \hat{L}(r) \tag{12}$$

$$\tau_a^{m,r} \geq 0 \quad \forall\, a \in \hat{L}(r) \tag{13}$$

$$e_a^{m,r} \geq 0 \quad \forall\, a \in A(r) \tag{14}$$

$$d_a^{m,r} \geq 0 \quad \forall\, a \in A(r) \tag{15}$$

$$E_i^{m,r} \geq 0 \quad \forall\, i \in N(r) \tag{16}$$

where E_{max}^m and E_0^m are respectively the battery size and initial battery level of class m PHET; b_{lo}^m and b_{up}^m are respectively the coefficients that determine the lower and upper bounds of the battery level; ε is the charging rate of the charging lanes; $E_i^{m,r}$ denotes the battery level of a class m PHET at node $i \in N$ along route $r \in R_m^w$; and $N(r)$ denotes the set of nodes of route r.

The solution of model P1 describes a class m PHET driver's optimal driving behavior and charging plan along a given route, to minimize his or her total travel cost. Constraint (1) ensures that the electricity and diesel consumptions on a link satisfy the energy consumption requirements. Constraints (2) and (3) specify the changes in the battery level on a link due to charging and discharging. Constraint (4) specifies the initial battery level. Constraints (5) and (6) ensure that the battery level is within a reserved range set by manufacturers to protect the battery. Constraints (7)–(9) describe the relationships among the charging time $\hat{\tau}_a^{m,r}$, actual travel time $\tau_a^{m,r}$, maximum travel time $\bar{t}_a$, and minimum travel time $t_a(v_a)$ on a candidate charging link. Constraints (10)–(11) set the upper bounds for $e_a^{m,r}$ and $d_a^{m,r}$, respectively. Constraints (12)–(16) are non-negativity constraints.

Equality constraints (1)–(4) can be relaxed to the following inequality constraints without affecting the optimal objective function value of P1:

$$e_a^{m,r} TWE^m + d_a^{m,r} TWD^m \geq \varpi_a^m \quad \forall\, a \in A(r) \tag{17}$$

$$E_j^{m,r} - E_i^{m,r} + e_a^{m,r} \leq 0 \quad \forall\, (i,j) = a \in L(r) \tag{18}$$

$$E_j^{m,r} - E_i^{m,r} + e_a^{m,r} - y_a \hat{\tau}_a^{m,r} \varepsilon \leq 0 \quad \forall\, (i,j) = a \in \hat{L}(r) \tag{19}$$

$$E_{O(w)}^{m,r} \leq E_0^m \tag{20}$$

Let P2 denote the program that is identical to P1 except that constraints (1)–(4) are replaced with constraints (17)–(20). By considering the fact that fuel cost is minimized in the objective function, it can be proved that the above relaxation will not change the optimal objective function value (see Appendix B for the proof). It should be noted that $E_i^{m,r}$ and $\hat{\tau}_a^{m,r}$ in P2 no longer have specific physical meaning, and they should only be regarded as auxiliary variables.

In the following, the network equilibrium model is formulated as a variational inequality (VI) and then reformulated as a non-linear program (NLP) using duality. Our motivation of conducting the relaxation comes from the fact that equality constraints are the most difficult to handle in NLP (Chinneck, 2006, Chapter 19). As pointed out by Chinneck (2006), it is difficult to find a point that lies exactly on multiple curved surfaces simultaneously in a high dimensional space.

For each route $r \in R_m^w$, $w \in W$, $m \in M1$, there is a corresponding P2 that determines the optimal operation of PHET drivers on the route. P2 is a linear program with the following optimality conditions:

(5)–(20) and

$$VOE + \eta_a^{m,r} TWE^m - \beta_a^{m,r} TWE^m + \chi_a^{m,r} \geq 0 \quad \forall\, a \in A(r) \tag{21}$$

$$(VOE + \eta_a^{m,r} TWE^m - \beta_a^{m,r} TWE^m + \chi_a^{m,r}) e_a^{m,r} = 0 \quad \forall\, a \in A(r) \tag{22}$$

$$VOD + \zeta_a^{m,r} TWD^m - \beta_a^{m,r} TWD^m \geq 0 \quad \forall\, a \in A(r) \tag{23}$$

$$(VOD + \zeta_a^{m,r} TWD^m - \beta_a^{m,r} TWD^m) d_a^{m,r} = 0 \quad \forall\, a \in A(r) \tag{24}$$

$$y_a VOT^m - \lambda_a^{m,r} + \mu_a^{m,r} - \xi_a^{m,r} \geq 0 \quad \forall\, a \in \hat{L}(r) \tag{25}$$

$$(y_a VOT^m - \lambda_a^{m,r} + \mu_a^{m,r} - \xi_a^{m,r}) \tau_a^{m,r} = 0 \quad \forall\, a \in \hat{L}(r) \tag{26}$$

$$\lambda_a^{m,r} - y_a \varepsilon \chi_a^{m,r} \geq 0 \quad \forall\, a \in \hat{L}(r) \tag{27}$$

$$(\lambda_a^{m,r} - y_a \varepsilon \chi_a^{m,r}) \hat{\tau}_a^{m,r} = 0 \quad \forall\, a \in \hat{L}(r) \tag{28}$$

$$-\chi_{ij}^{m,r} + \chi_{ki}^{m,r} + \psi_i^{m,r} - \omega_i^{m,r} \geq 0 \quad \forall\, (i,j), (k,i) \in A(r),\ i \notin \{O(w), D(w)\} \tag{29}$$

$$(-\chi_{ij}^{m,r} + \chi_{ki}^{m,r} + \psi_i^{m,r} - \omega_i^{m,r}) E_i^{m,r} = 0 \quad \forall\, (i,j), (k,i) \in A(r),\ i \notin \{O(w), D(w)\} \tag{30}$$

$$-\chi_{O(w)j}^{m,r} + \psi_{O(w)}^{m,r} - \omega_{O(w)}^{m,r} + \alpha_{O(w)}^{m,r} \geq 0 \quad \forall\, (O(w), j) = a \in A(r) \tag{31}$$

$$(-\chi_{O(w)j}^{m,r} + \psi_{O(w)}^{m,r} - \omega_{O(w)}^{m,r} + \alpha_{O(w)}^{m,r}) E_{O(w)}^{m,r} = 0 \quad \forall\, (O(w), j) = a \in A(r) \tag{32}$$

$$\chi_{kD(w)}^{m,r} + \psi_{D(w)}^{m,r} - \omega_{D(w)}^{m,r} \geq 0 \quad \forall\, (k, D(w)) = a \in A(r) \tag{33}$$

$$(\chi_{kD(w)}^{m,r} + \psi_{D(w)}^{m,r} - \omega_{D(w)}^{m,r}) E_{D(w)}^{m,r} = 0 \quad \forall (k, D(w)) = a \in A(r) \tag{34}$$

$$(\hat{\tau}_a^{m,r} - \tau_a^{m,r}) \lambda_a^{m,r} = 0 \quad \forall a \in \hat{L}(r) \tag{35}$$

$$(\tau_a^{m,r} - \bar{t}_a) \mu_a^{m,r} = 0 \quad \forall a \in \hat{L}(r) \tag{36}$$

$$(t_a(v_a) - \tau_a^{m,r}) \xi_a^{m,r} = 0 \quad \forall a \in \hat{L}(r) \tag{37}$$

$$(e_a^{m,r} TWE^m - \varpi_a^m) \eta_a^{m,r} = 0 \quad \forall a \in A(r) \tag{38}$$

$$(d_a^{m,r} TWD^m - \varpi_a^m) \zeta_a^{m,r} = 0 \quad \forall a \in A(r) \tag{39}$$

$$(E_i^{m,r} - E_{max}^m b_{up}^m) \psi_i^{m,r} = 0 \quad \forall i \in N(r) \tag{40}$$

$$(E_i^{m,r} - E_{max}^m b_{lo}^m) \omega_i^{m,r} = 0 \quad \forall i \in N(r) \tag{41}$$

$$(e_a^{m,r} TWE^m + d_a^{m,r} TWD^m - \varpi_a^m) \beta_a^{m,r} = 0 \quad \forall a \in A(r) \tag{42}$$

$$(E_j^{m,r} - E_i^{m,r} + e_a^{m,r}) \chi_{ij}^{m,r} = 0 \quad \forall (i, j) = a \in L(r) \tag{43}$$

$$(E_j^{m,r} - E_i^{m,r} + e_a^{m,r} - y_a \hat{\tau}_a^{m,r} \varepsilon) \chi_{ij}^{m,r} = 0 \quad \forall (i, j) = a \in \hat{L}(r) \tag{44}$$

$$(E_{O(w)}^{m,r} - E_0^m) \alpha_{O(w)}^{m,r} = 0 \tag{45}$$

$$\lambda_a^{m,r} \geq 0 \quad \forall a \in \hat{L}(r) \tag{46}$$

$$\mu_a^{m,r} \geq 0 \quad \forall a \in \hat{L}(r) \tag{47}$$

$$\xi_a^{m,r} \geq 0 \quad \forall a \in \hat{L}(r) \tag{48}$$

$$\eta_a^{m,r} \geq 0 \quad \forall a \in A(r) \tag{49}$$

$$\zeta_a^{m,r} \geq 0 \quad \forall a \in A(r) \tag{50}$$

$$\psi_i^{m,r} \geq 0 \quad \forall i \in N(r) \tag{51}$$

$$\omega_i^{m,r} \geq 0 \quad \forall i \in N(r) \tag{52}$$

$$\beta_a^{m,r} \geq 0 \quad \forall a \in A(r) \tag{53}$$

$$\chi_{ij}^{m,r} \geq 0 \quad \forall (i, j) = a \in L(r) \tag{54}$$

$$\alpha_{O(w)}^{m,r} \geq 0 \tag{55}$$

where $\psi_i^{m,r}$, $\omega_i^{m,r}$, $\lambda_a^{m,r}$, $\mu_a^{m,r}$, $\xi_a^{m,r}$, $\eta_a^{m,r}$, $\zeta_a^{m,r}$, $\beta_a^{m,r}$, and $\alpha_{O(w)}^{m,r}$ are the multipliers corresponding to constraints (5)–(11), (17) and (20), respectively; and $\chi_a^{m,r}$ is the multiplier corresponding to constraints (18) and (19).

3.4. Network equilibrium model

As noted in assumption II in Section 2 regarding route choice, when choosing their routes, drivers attempt to minimize the total travel cost; for PHETs, the travel cost is determined by the travel time and fuel cost, while for other vehicles, the travel time is the only concern. Thus under UE, for each O-D pair and each user class, the total travel costs on all utilized routes are equal, and are less than or equal to the total travel cost that would be incurred on any unutilized route. The multi-class multi-criteria user equilibrium (MMUE) problem can be formulated as a nonlinear complementarity problem (NCP) as below. It should be noted that the UE conditions are for a given charging link configuration, i.e., holding $\{\cdots, y_a, \cdots\}$ constant. For completeness, we repeat some previously presented constraints here.

MMUE-NCP:

(5)–(55) and

$$\sum_{r \in R_m^w} f_r^m = q_m^w \quad \forall w \in W, m \in M \tag{56}$$

$$h_a^m = \sum_{w \in W} \sum_{r \in R_m^w} f_r^m \delta_a^r \quad \forall a \in A, m \in M \tag{57}$$

$$v_a = \sum_{m \in M} h_a^m \gamma^m \quad \forall a \in A \tag{58}$$

$$c_a^{m,r} = t_a(v_a)VOT^m + e_a^{m,r}VOE + d_a^{m,r}VOD \quad \forall a \in L(r), r \in R_m^w, w \in W, m \in M1 \tag{59}$$

$$c_a^{m,r} = ((1-y_a)t_a(v_a) + y_a\tau_a^{m,r})VOT^m + e_a^{m,r}VOE + d_a^{m,r}VOD \quad \forall a \in \hat{L}(r), r \in R_m^w, w \in W, m \in M1 \tag{60}$$

$$c_a^{m,r} = t_a(v_a)VOT^m \quad \forall a \in A(r), r \in R_m^w, w \in W, m \in M2 \tag{61}$$

$$f_r^m \geq 0 \quad \forall r \in R_m^w, w \in W, m \in M \tag{62}$$

$$\left(\sum_{a\in A(r)} c_a^{m,r} - \pi_m^w\right) f_r^m = 0 \quad \forall r \in R_m^w, w \in W, m \in M \tag{63}$$

$$\sum_{a\in A(r)} c_a^{m,r} - \pi_m^w \geq 0 \quad \forall r \in R_m^w, w \in W, m \in M \tag{64}$$

where π_m^w is an auxiliary variable representing the equilibrium travel cost of class $m \in M$ users between O-D pair $w \in W$. It should be noted that constraints (5)–(55) should be satisfied for $\forall r \in R_m^w$, $w \in W$, $m \in M1$, and that travel cost is in monetary unit.

The problem MMUE-NCP can be equivalently formulated as a variational inequality (VI). Define a set $\Phi = \{(\boldsymbol{\beta}, \boldsymbol{\chi}, \boldsymbol{\lambda}, \boldsymbol{\mu}, \boldsymbol{\xi}, \boldsymbol{\eta}, \boldsymbol{\zeta}, \boldsymbol{\psi}, \boldsymbol{\omega}, \boldsymbol{\alpha}, \boldsymbol{f}, \boldsymbol{h}, \boldsymbol{v}, \boldsymbol{e}, \boldsymbol{d}, \boldsymbol{\tau}, \hat{\boldsymbol{\tau}}, \boldsymbol{E})\}$, where the vector satisfies equations (12)–(16) and (46)–(62). The solution to the following VI, i.e., $(\boldsymbol{\beta}^*, \boldsymbol{\chi}^*, \boldsymbol{\lambda}^*, \boldsymbol{\mu}^*, \boldsymbol{\xi}^*, \boldsymbol{\eta}^*, \boldsymbol{\zeta}^*, \boldsymbol{\psi}^*, \boldsymbol{\omega}^*, \boldsymbol{\alpha}^*, \boldsymbol{f}^*, \boldsymbol{h}^*, \boldsymbol{v}^*, \boldsymbol{e}^*, \boldsymbol{d}^*, \boldsymbol{\tau}^*, \hat{\boldsymbol{\tau}}^*, \boldsymbol{E}^*) \in \Phi$, also solves the MMUE-NCP.

MMUE-VI:

$$\begin{aligned}
&\sum_{w\in W}\sum_{m\in M1}\sum_{r\in R_m^w}\Bigg[\sum_{i\in N(r)}[(E_{max}^m b_{up}^m - E_i^{m,r*})(\psi_i^{m,r} - \psi_i^{m,r*}) + (E_i^{m,r*} - E_{max}^m b_{lo}^m)(\omega_i^{m,r} - \omega_i^{m,r*})] \\
&\quad - \sum_{a\in\hat{L}(r)}[(\hat{\tau}_a^{m,r*} - \tau_a^{m,r*})(\lambda_a^{m,r} - \lambda_a^{m,r*}) + (\tau_a^{m,r*} - \bar{t}_a)(\mu_a^{m,r} - \mu_a^{m,r*}) + (t_a{}^* - \tau_a^{m,r*})(\xi_a^{m,r} - \xi_a^{m,r*})] \\
&\quad + \sum_{a\in A(r)}[(e_a^{m,r*}TWE^m + d_a^{m,r*}TWD^m - \varpi_a^m)(\beta_a^{m,r} - \beta_a^{m,r*}) - (e_a^{m,r*}TWE^m - \varpi_a^m)(\eta_a^{m,r} - \eta_a^{m,r*}) - (d_a^{m,r*}TWD^m - \varpi_a^m)(\zeta_a^{m,r} - \zeta_a^{m,r*})] \\
&\quad - \sum_{a\in A(r)}(E_j^{m,r*} - E_i^{m,r*} + e_a^{m,r*})(\chi_a^{m,r} - \chi_a^{m,r*}) - \sum_{a\in\hat{L}(r)}(-y_a\hat{\tau}_a^{m,r*}\varepsilon)(\chi_a^{m,r} - \chi_a^{m,r*}) - (E_{O(w)}^{m,r*} - E_0^m)(\alpha_{O(w)}^{m,r} - \alpha_{O(w)}^{m,r*}) + \alpha_{O(w)}^{m,r*}(E_{O(w)}^{m,r} - E_{O(w)}^{m,r*}) \\
&\quad + \sum_{i\in N(r)}(\psi_i^{m,r*} - \omega_i^{m,r*})(E_i^{m,r} - E_i^{m,r*}) + \sum_{(i,j)\in A(r)}[-\chi_{ij}^{m,r*}(E_i^{m,r} - E_i^{m,r*}) + \chi_{ij}^{m,r*}(E_j^{m,r} - E_j^{m,r*})] \\
&\quad + \sum_{a\in A(r)}[(VOE + \eta_a^{m,r*}TWE^m - \beta_a^{m,r*}TWE^m + \chi_a^{m,r*})(e_a^{m,r} - e_a^{m,r*}) + (VOD + \zeta_a^{m,r*}TWD^m - \beta_a^{m,r*}TWD^m)(d_a^{m,r} - d_a^{m,r*})] \\
&\quad + \sum_{a\in\hat{L}(r)}[(y_a VOT^m - \lambda_a^{m,r*} + \mu_a^{m,r*} - \xi_a^{m,r*})(\tau_a^{m,r} - \tau_a^{m,r*}) + (\lambda_a^{m,r*} - y_a\varepsilon\chi_a^{m,r*})(\hat{\tau}_a^{m,r} - \hat{\tau}_a^{m,r*})]\Bigg] \\
&\quad + \sum_{w\in W}\sum_{m\in M}\sum_{r\in R_m^w}\sum_{a\in A(r)} c_a^{m,r*}(f_r^m - f_r^{m*}) \geq 0, \forall (\boldsymbol{\beta}, \boldsymbol{\chi}, \boldsymbol{\lambda}, \boldsymbol{\mu}, \boldsymbol{\xi}, \boldsymbol{\eta}, \boldsymbol{\zeta}, \boldsymbol{\psi}, \boldsymbol{\omega}, \boldsymbol{\alpha}, \boldsymbol{f}, \boldsymbol{h}, \boldsymbol{v}, \boldsymbol{e}, \boldsymbol{d}, \boldsymbol{\tau}, \hat{\boldsymbol{\tau}}, \boldsymbol{E}) \in \Phi
\end{aligned}$$

The equivalence can be easily established by deriving the Karush–Kuhn–Tucker (KKT) conditions of the MMUE-VI above and comparing them with the MMUE-NCP.

Even for strictly monotone link performance functions, the MMUE problem may have non-unique solutions for the aggregate link flow distribution and the O-D equilibrium travel cost. An example is provided to demonstrate such a non-uniqueness property. Let us consider a toy network with three nodes, three links (all charging links), two O-D pairs (1,2) and (1,3), and three routes, as shown in Fig. 1. The relevant parameters are as follows:

(a) User class set: $M1 = \{1\}$, $M2 = \{2\}$, where classes 1 and 2 are PHET users and passenger car users, respectively.

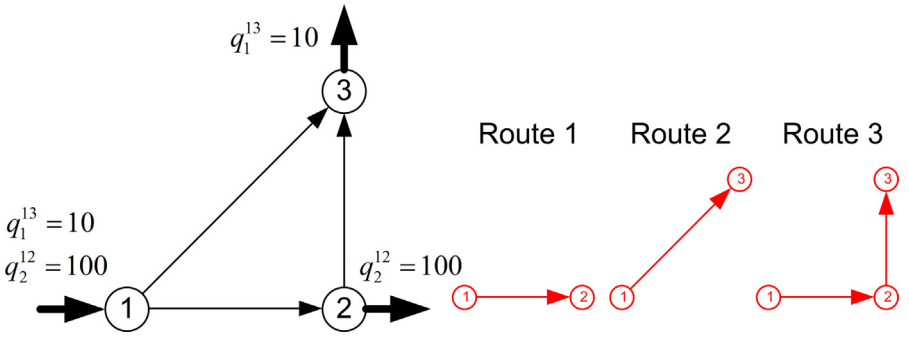

Fig. 1. Illustration of the routes of a network comprising two O-D pairs.

Table 1
Flow distributions and O-D equilibrium travel costs for the network comprising two O-D pairs.

Link	Flow (h_{ij}^1, h_{ij}^2; v_{ij})	Minimum travel time	Specific contents for PHETs				O-D travel cost
			Actual travel time	Charging time	Energy consumption ($e_a^{1,r}$, $d_a^{1,r}$)	Fuel cost	
MMUE solution 1							
(1,2)	(1, 100; 102)	56	60	60	(75, 0)	75	–
(1,3)	(9, 0; 18)	33	100	100	(150, 0)	150	–
(2,3)	(1, 0; 2)	6	40	40	(75, 0)	75	–
Route	(f_r^1, f_r^2)				($\Sigma e_a^{1,r}$, $\Sigma d_a^{1,r}$)		
1 (1–2)	(0, 100)	56	–	–	–	–	56
2 (1–3)	(9, 0)	33	100	100	(150, 0)	150	350
3 (1–2-3)	(1, 0)	62	100	100	(150, 0)	150	350
MMUE solution 2							
(1,2)	(9, 100; 118)	64	75	75	(75, 0)	75	–
(1,3)	(1, 2; 2)	17	100	100	(150, 0)	150	–
(2,3)	(9, 0; 18)	14	25	25	(75, 0)	75	–
Route	(f_r^1, f_r^2)				($\Sigma e_a^{1,r}$, $\Sigma d_a^{1,r}$)		
1 (1–2)	(0, 100)	64	–	–	–	–	64
2 (1–3)	(1, 0)	17	100	100	(150, 0)	150	350
3 (1–2-3)	(9, 0)	78	100	100	(150, 0)	150	350

(b) Demand: $q_1^{12} = 0$, $q_2^{12} = 100$, $q_1^{13} = 10$, $q_2^{13} = 0$
(c) PCE conversion factors: $\gamma^1 = 2.0$, $\gamma^2 = 1.0$
(d) Link performance function: $t_{12}(v_{12}) = 5 + 0.5v_{12}$, $t_{13}(v_{13}) = 15 + v_{13}$, $t_{23}(v_{23}) = 5 + 0.5v_{23}$
(e) Energy consumption: $\varpi_{12}^1 = 300$, $\varpi_{23}^1 = 300$, $\varpi_{13}^1 = 600$
(f) Energy efficiency: $TWE^1 = 4$, $TWD^1 = 1$
(g) Unit energy cost: $VOE = 1$, $VOD = 1$
(h) Value of time: $VOT^1 = 2$, $VOT^2 = 1$
(i) Battery parameter: $E_{max}^1 = 50$, $b_{up}^1 = 1$, $b_{lo}^1 = 0$, E_0^1=50
(j) Charging rate on charging link: $\varepsilon = 1$

As indicated in Table 1, two different sets of aggregate link flows (v_{12}, v_{13}, v_{23})= (102, 18, 2) and (118, 2, 18) both satisfy the MMUE conditions. For the former, the calculated minimum travel times on routes 1, 2, and 3, based on the link performance functions, are 56, 33 and 62, respectively. However, the actual travel times of a PHET driver on routes 2 and 3 (equal to the respective charging times) are both 100, which minimize the total travel costs. For the latter solution, the calculated travel times on routes 1, 2, and 3 are 64, 17 and 78, respectively. Once again, a PHET driver on routes 2 and 3 will choose to slow down to gain more energy, resulting in an actual travel and charging time of 100 on both routes. Further, the two MMUE solutions have identical PHET travel costs for O-D pair (1,3), but yield different passenger car travel costs for O-D pair (1,2). The implied non-uniqueness of the aggregate link flow and O-D equilibrium travel cost is mainly due to two factors: (1) the speed choice behavior of PHET drivers, and (2) the bi-criteria route choice behaviors of PHET drivers. In the literature, Chen et al. (2016) considered the speed choice behavior of battery electric vehicles in a network with charging lanes and also proposed a UE model with non-unique link flow solutions; Nagurney (2000) identified that a general multi-class multi-criteria UE problem may have non-unique link flow solutions.

3.5. Solution procedure

MMUE-VI was solved by the technique developed by Aghassi et al. (2006), whereby duality was used to reformulate the MMUE-VI as the following nonlinear program (NLP):

MMUE-NLP:

$$\min_{(\boldsymbol{\beta},\boldsymbol{\chi},\boldsymbol{\lambda},\boldsymbol{\mu},\boldsymbol{\xi},\boldsymbol{\eta},\boldsymbol{\zeta},\boldsymbol{\psi},\boldsymbol{\omega},\boldsymbol{\alpha},\boldsymbol{f},\boldsymbol{h},\boldsymbol{v},\boldsymbol{e},\boldsymbol{d},\boldsymbol{\tau},\hat{\boldsymbol{\tau}},\boldsymbol{E},\boldsymbol{\pi})} \sum_{w\in W}\sum_{m\in M1}\sum_{r\in R_m^w}\Bigg[\sum_{i\in N(r)}[(E_{max}^m b_{up}^m - E_i^{m,r})\psi_i^{m,r} + (E_i^{m,r} - E_{max}^m b_{lo}^m)\omega_i^{m,r}]$$
$$- \sum_{a\in\hat{L}(r)}[(\hat{\tau}_a^{m,r} - \tau_a^{m,r})\lambda_a^{m,r} + (\tau_a^{m,r} - \bar{l}_a)\mu_a^{m,r} + (t_a - \tau_a^{m,r})\xi_a^{m,r}] + \sum_{a\in A(r)}[(e_a^{m,r}TWE^m + d_a^{m,r}TWD^m - \varpi_a^m)\beta_a^{m,r} - (e_a^{m,r}TWE^m - \varpi_a^m)\eta_a^{m,r} - (d_a^{m,r}TWD^m - \varpi_a^m)\zeta_a^{m,r}]$$
$$- \sum_{a\in A(r)}(E_j^{m,r} - E_i^{m,r} + e_a^{m,r})\chi_a^{m,r} - \sum_{a\in\hat{L}(r)}(-y_a\hat{\tau}_a^{m,r}\varepsilon)\chi_a^{m,r} - (E_{O(w)}^{m,r} - E_0^m)\alpha_{O(w)}^{m,r} + \alpha_{O(w)}^{m,r}E_{O(w)}^{m,r} + \sum_{i\in N(r)}(\psi_i^{m,r} - \omega_i^{m,r})E_i^{m,r} + \sum_{(i,j)\in A(r)}(-\chi_{ij}^{m,r}E_i^{m,r} + \chi_{ij}^{m,r}E_j^{m,r})$$
$$+ \sum_{a\in A(r)}[(VOE + \eta_a^{m,r}TWE^m - \beta_a^{m,r}TWE^m + \chi_a^{m,r})e_a^{m,r} + (VOD + \zeta_a^{m,r}TWD^m - \beta_a^{m,r}TWD^m)d_a^{m,r}]$$
$$+ \sum_{a\in\hat{L}(r)}[(y_a VOT^m - \lambda_a^{m,r} + \mu_a^{m,r} - \xi_a^{m,r})\tau_a^{m,r} + (\lambda_a^{m,r} - y_a\varepsilon\chi_a^{m,r})\hat{\tau}_a^{m,r}]\Bigg] + \sum_{w\in W}\sum_{m\in M}\sum_{r\in R_m^w}\sum_{a\in A(r)}c_a^{m,r}f_r^m - \sum_{w\in W}\sum_{m\in M}q_m^w\pi_m^w$$

s.t.

(5)–(11), (17)–(21), (23), (25), (27), (29), (31), (33) $\quad \forall\, r \in R_m^w,\, w \in W,\, m \in M1$

$\pi_m^w \le \sum_{a \in A(r)} c_a^{m,r} \quad \forall\, r \in R_m^w,\, w \in W,\, m \in M$

$(\boldsymbol{\beta}, \boldsymbol{\chi}, \boldsymbol{\lambda}, \boldsymbol{\mu}, \boldsymbol{\xi}, \boldsymbol{\eta}, \boldsymbol{\zeta}, \boldsymbol{\psi}, \boldsymbol{\omega}, \boldsymbol{\alpha}, \boldsymbol{f}, \boldsymbol{h}, \boldsymbol{v}, \boldsymbol{e}, \boldsymbol{d}, \boldsymbol{\tau}, \hat{\boldsymbol{\tau}}, \boldsymbol{E}) \in \Phi$

The objective function of the above MMUE-NLP problem is to minimize the gap between a primal and dual problem associated with MMUE-VI, and the constraints are those from the primal and dual problems. In solving the MMUE-NLP problem, if the value of the optimal objective function is zero, then one part of the optimal solution, $(\boldsymbol{\beta}, \boldsymbol{\chi}, \boldsymbol{\lambda}, \boldsymbol{\mu}, \boldsymbol{\xi}, \boldsymbol{\eta}, \boldsymbol{\zeta}, \boldsymbol{\psi}, \boldsymbol{\omega}, \boldsymbol{\alpha}, \boldsymbol{f}, \boldsymbol{h}, \boldsymbol{v}, \boldsymbol{e}, \boldsymbol{d}, \boldsymbol{\tau}, \hat{\boldsymbol{\tau}}, \boldsymbol{E})$, would be the solution to the MMUE-VI problem.

Because an MMUE-NLP model is a regular nonlinear program, it can be easily solved using a commercial nonlinear solver such as CONOPT (Drud, 1994). However, an MMUE-NLP model is path-flow-based and thus requires prior path enumeration. The column generation algorithm developed by Leventhal et al. (1973) was used to efficiently solve the MMUE-NLP problem of a large-scale network in the present study. An iterative solution procedure was adopted. Beginning with any subset of R_m^w, $m \in M$, $w \in W$, a restricted version of the MMUE-NLP problem was solved over the subset. Based on the obtained solution, a series of shortest-path sub-problems were solved to determine whether the solution of the restricted MMUE-NLP problem applied to the original formulation. If not, new routes generated from the sub-problems were added to the route subset and the iteration proceeded until termination.

Considering the different routing criteria of PHETs and other vehicles, it was necessary to formulate two different shortest-path sub-problems. For this purpose, we first introduced some new parameters. Let Δ denote the node-link incidence matrix of the network; let Ψ^wdenote an "input-output" vector with exactly two non-zero components: one has a value of 1 corresponding to the origin node of the O-D pair w, and the other has a value of -1 corresponding to the destination node of w. For each class $m \in M2$ and each O-D pair $w \in W$, the formulation of the shortest-path problem is as follows:

SP-M2:

$$\min_{\boldsymbol{x}} \sum_{a \in A} t_a(v_a) x_a^{m,w}$$

$s.\ t.$

$$\Delta \boldsymbol{x}^{m,w} = \Psi^w \tag{65}$$

$$x_a^{m,w} \in \{0, 1\} \quad \forall\, a \in A \tag{66}$$

where $x_a^{m,w}$ is a binary variable, equal to 1 if a link a is utilized, and 0 if otherwise.

Problem SP-M2 is an integer linear program that can be easily solved by a commercial solver such as CPLEX 12.2. The well-known Dijkstra algorithm (Dijkstra,1959) can also be used to efficiently solve the problem.

For each class $m \in M1$ and each O-D pair $w \in W$, the formulation of the shortest-path problem is as follows:

SP-M1:

$$\min_{\boldsymbol{x},\boldsymbol{u},\boldsymbol{e},\boldsymbol{d},\boldsymbol{\tau},\hat{\boldsymbol{\tau}},\boldsymbol{E}} \sum_{a \in \hat{L}} \{[(1-y_a) t_a(v_a) + y_a \tau_a^{m,w}] VOT^m + e_a^{m,w} VOE + d_a^{m,w} VOD\} x_a^{m,w} + \sum_{a \in L} (t_a(v_a) VOT^m + e_a^{m,w} VOE + d_a^{m,w} VOD) x_a^{m,w}$$

$s.\ t.$

$$\Delta \boldsymbol{x}^{m,w} = \Psi^w \tag{67}$$

$$\hat{\tau}_a^{m,w} - \tau_a^{m,w} \le 0 \quad \forall\, a \in \hat{L} \tag{68}$$

$$\tau_a^{m,w} - \bar{t}_a \le 0 \quad \forall\, a \in \hat{L} \tag{69}$$

$$t_a(v_a) - \tau_a^{m,w} \le 0 \quad \forall\, a \in \hat{L} \tag{70}$$

$$e_a^{m,w} TWE^m + d_a^{m,w} TWD^m = \varpi_a^m \quad \forall\, a \in A \tag{71}$$

$$E_j^{m,w} - E_i^{m,w} + e_a^{m,w} = u_a^{m,w} \quad \forall\, (i,j) = a \in L \tag{72}$$

$$E_j^{m,w} - E_i^{m,w} + e_a^{m,w} - y_a \hat{\tau}_a^{m,w} \varepsilon = u_a^{m,w} \quad \forall\, (i,j) = a \in \hat{L} \tag{73}$$

$$u_a^{m,w} \le K_1 (1 - x_a^{m,w}) \quad \forall\, a \in A \tag{74}$$

$$u_a^{m,w} \ge -K_1 (1 - x_a^{m,w}) \quad \forall\, a \in A \tag{75}$$

$$E_i^{m,w} \le E_{max}^m b_{up}^m \quad \forall\, i \in N \tag{76}$$

$$E_i^{m,w} \ge E_{max}^m b_{lo}^m \quad \forall\, i \in N \tag{77}$$

$$E_{O(w)}^{m,w} = E_0^m \tag{78}$$

$$\hat{\tau}_a^{m,w} \ge 0 \quad \forall\, a \in \hat{L} \tag{79}$$

$$e_a^{m,w} \geq 0 \quad \forall\, a \in A \tag{80}$$

$$d_a^{m,w} \geq 0 \quad \forall\, a \in A \tag{81}$$

$$x_a^{m,w} \in \{0, 1\} \quad \forall\, a \in A \tag{82}$$

where $x_a^{m,w}$ is a binary variable, equal to 1 if link a is utilized, and otherwise 0; K_1 is a sufficiently large constant; $u_a^{m,w}$ is a variable, equal to 0 if link a is utilized, and otherwise unrestricted; $e_a^{m,w}$ and $d_a^{m,w}$ are respectively the electricity and diesel consumptions of a PHET on link a; $\tau_a^{m,w}$ and $\hat{\tau}_a^{m,w}$ are respectively the actual travel time and charging time of a PHET on link a; and $E_i^{m,w}$ is the battery level of a PHET at node i.

In the above formulation, the objective function is to minimize the generalized total travel cost of PHETs. Constraint (67) ensures flow balance. Constraints (68)–(70) describe the relationship among the charging time $\hat{\tau}_a^{m,w}$, actual travel time $\tau_a^{m,w}$, maximum travel time $\bar{t}_a$, and minimum travel time $t_a(v_a)$ on the candidate charging links. Constraint (71) ensures that the electricity and diesel consumptions on a link satisfy the energy consumption requirements. Constraints (72)–(75) specify the changes in the battery level on a utilized link due to charging and discharging. Constraints (76) and (77) ensure that the battery level is always within a prescribed range set by the manufacturers to protect the battery. Constraint (78) specifies the initial battery level. Constraints (79)–(81) ensure that the actual charging time, electricity consumption, and diesel consumption on a link cannot be negative. Finally, constraint (82) ensures that $x_a^{m,w}$ is binary.

SP-M1 is a mixed integer nonlinear program that cannot be easily solved, especially for a large network. Through the introduction of a new variable $z_a^{m,w}$ to replace the nonlinear portion of the objective function of SP-M1, i.e., $(y_a\tau_a^{m,w}VOT^m + e_a^{m,w}VOE + d_a^{m,w}VOD)x_a^{m,w}$ for $a \in \hat{L}$ and $(e_a^{m,w}VOE + d_a^{m,w}VOD)x_a^{m,w}$ for $a \in L$, the SP-M1 can be equivalently reformulated as the following linear program:

L-SP-M1:

$$\min_{\boldsymbol{x},\boldsymbol{u},\boldsymbol{e},\boldsymbol{d},\boldsymbol{\tau},\hat{\boldsymbol{\tau}},\boldsymbol{E},\boldsymbol{z}} \sum_{a\in A} z_a^{m,w} + \sum_{a\in\hat{L}} (1-y_a)t_a(v_a)VOT^m x_a^{m,w} + \sum_{a\in L} t_a(v_a)VOT^m x_a^{m,w}$$

s. t. (67)–(82)

$$z_a^{m,w} \leq e_a^{m,w}VOE + d_a^{m,w}VOD \quad \forall\, a \in L \tag{83}$$

$$z_a^{m,w} \leq y_a\tau_a^{m,w}VOT^m + e_a^{m,w}VOE + d_a^{m,w}VOD \quad \forall\, a \in \hat{L} \tag{84}$$

$$z_a^{m,w} \geq K_1(x_a^{m,w}-1) + e_a^{m,w}VOE + d_a^{m,w}VOD \quad \forall\, a \in L \tag{85}$$

$$z_a^{m,w} \geq K_1(x_a^{m,w}-1) + y_a\tau_a^{m,w}VOT^m + e_a^{m,w}VOE + d_a^{m,w}VOD \quad \forall\, a \in \hat{L} \tag{86}$$

$$z_a^{m,w} \leq K_1 x_a^{m,w} \quad \forall\, a \in A \tag{87}$$

$$z_a^{m,w} \geq 0 \quad \forall\, a \in A \tag{88}$$

L-SP-M1 is a mixed integer linear program that can be solved by a commercial solver such as CPLEX 12.2. Given a set of aggregate link flow solutions $\{\cdots,v_a,\cdots\}$ of a restricted MMUE-NLP problem, SP-M2 and L-SP-M1 can be solved for each class and each O-D pair. The optimal solution of SP-M2, denoted by $\tilde{\boldsymbol{x}}^{m,w}$, can be used to construct the shortest path for class $m \in M2$ users, denoted as $\tilde{r}_m^w$; and the optimal solution of L-SP-M1, denoted by $\tilde{\boldsymbol{x}}^{m,w}$, can be used to obtain the shortest path for class $m \in M1$ users, denoted by $\tilde{r}_m^w$. The iterative procedure for solving the MMUE-NLP problem is as follows:

Step 0: Set $\{\cdots,v_a,\cdots\} = 0$. For each O-D pair $w \in W$, solve SP-M2 for class $m \in M2$ users and solve L-SP-M1 for class $m \in M1$ users. Construct $\widetilde{R}_m^w = \{\tilde{r}_m^w\}$.

Step 1: Solve the MMUE-NLP problem over $\cup_{w\in W}\cup_{m\in M}\widetilde{R}_m^w$ and obtain the link flow distribution $\{\cdots,v_a,\cdots\}$ and the multipliers associated with constraints $\sum_{r\in\widetilde{R}_m^w} f_r^m = q_m^w$, denoted as ρ_m^w, $\forall\, w \in W$.

Step 2: For each O-D pair $w \in W$, solve SP-M2 for each class $m \in M2$, solve L-SP-M1 for each class $m \in M1$, and construct routes $\tilde{r}_m^w$ for each class $m \in M$. If for each O-D pair $w \in W$, $\sum_{a\in A(\tilde{r}_m^w)} t_a(v_a)VOT^m x_a^{m,w} \geq \rho_m^w$ for each class $m \in M2$ and $\sum_{a\in A(\tilde{r}_m^w)} z_a^{m,w} + \sum_{a\in\hat{L}(\tilde{r}_m^w)}(1-y_a)t_a(v_a)VOT^m x_a^{m,w} + \sum_{a\in L(\tilde{r}_m^w)} t_a(v_a)VOT^m x_a^{m,w} \geq \rho_m^w$ for each class $m \in M1$, then terminate; the current solution of the restricted MMUE-NLP problem is the UE solution. Otherwise, add all the routes $\tilde{r}_m^w$ for class $m \in M2$ that satisfy $\sum_{a\in A(\tilde{r}_m^w)} t_a(v_a)VOT^m x_a^{m,w} < \rho_m^w$, and the routes $\tilde{r}_m^w$ for class $m \in M1$ that satisfy $\sum_{a\in A(\tilde{r}_m^w)} z_a^{m,w} + \sum_{a\in\hat{L}(\tilde{r}_m^w)}(1-y_a)t_a(v_a)VOT^m x_a^{m,w} + \sum_{a\in L(\tilde{r}_m^w)} t_a(v_a)VOT^m x_a^{m,w} < \rho_m^w$ to $\widetilde{R}_m^w$, and return to Step 1.

4. Deployment of charging lanes for PHETs

In this section, the optimal deployment of charging lanes in a general network with limited budget is investigated. The problem is considered as a generalized bi-level NDP, where the upper-level problem deploys charging lanes in the network and the lower-level problem determines the route choice behavior of road users. The objective of the upper-level problem, i.e., the system performance measure, is first presented. The impact of non-unique UE solutions on the evaluation of system performance is then discussed. Lastly, the charging lane deployment problem is formulated as a mathematical program.

4.1. Objective of the upper-level problem

The upper-level problem seeks to determine which links to be converted into charging lanes to optimize the system performance. In this study, total cost (*TC*) is used as the system performance measure. It consists of the total system travel time cost (*TSTC*), total fuel cost (*TFC*), and total emission cost (*TEC*). *TSTC* and *TFC* are direct costs of transportation, while *TEC* is an external cost. The system performance function is given by

$$TC = \Omega_1 \times TSTC + \Omega_2 \times TFC + \Omega_3 \times TEC$$

where Ω_1, Ω_2, and Ω_3 are the weight of *TSTC*, *TFC*, and *TEC* in the *TC*, respectively. These three weights are dependent on planners' experience, experts' judgment, as well as the decision makers' preference.

4.1.1. Total system travel time cost

The *TSTC* is defined by summing up the product of the total travel time and the value of time (*VOT*) for all user classes

$$\begin{aligned} TSTC = & \sum_{w\in W} \sum_{m\in M1} \sum_{r\in R_m^w} \left[\sum_{a\in L(r)} t_a + \sum_{a\in \hat{L}(r)} ((1-y_a)t_a + y_a \tau_a^{m,r}) \right] VOT^m f_r^m \\ & + \sum_{w\in W} \sum_{m\in M2} \sum_{r\in R_m^w} \sum_{a\in A(r)} VOT^m t_a f_r^m \end{aligned} \tag{89}$$

4.1.2. Total fuel cost

The *TFC* is defined by summing up the product of total fuel consumption and the value of fuel (*VOF*) for electricity and fossil fuel

$$TFC = \sum_{w\in W} \sum_{m\in M1} \sum_{r\in R_m^w} \sum_{a\in A(r)} (e_a^{m,r} VOE + d_a^{m,r} VOD) f_r^m \tag{90}$$

4.1.3. Total emission cost

The *TEC* is defined by summing up the emission cost EC_l of each pollutant l

$$TEC = \sum_l EC_l \tag{91}$$

Four key pollutants are considered for calculating the emission cost: carbon monoxide (CO), hydrocarbons (HC), nitrogen oxides (NO_x), and particulate matter (PM). For simplicity, we adopt a fuel-based method proposed by Dreher and Harley (1998) to estimate truck emissions. Let EI_l represent the emission index for pollutant l, in units of mass of pollutant l emitted per unit volume of fuel consumed. EI_l is given by

$$EI_l = \frac{BSPE_l}{BSFC} \tag{92}$$

where $BSPE_l$ is the brake specific pollutant emission factor obtained from the dynamometer test, expressed in g/kWh units; and BSFC is the brake specific fuel consumption of the diesel engine, in gallon/kWh. The emission cost EC_l can then be given by

$$EC_l = \varrho_l \times EI_l \times \frac{1}{\vartheta} \times \sum_{w\in W} \sum_{m\in M1} \sum_{r\in R_m^w} \sum_{a\in A(r)} d_a^{m,r} f_r^m \tag{93}$$

where ϱ_l is the external cost per unit mass of pollutant l, ϑ is the heat content of diesel, and $\sum_{w\in W} \sum_{m\in M1} \sum_{r\in R_m^w} \sum_{a\in A(r)} d_a^{m,r} f_r^m$ is the total diesel consumption in kWh/h units.

4.2. Discussion of non-uniqueness of MMUE

As noted in Section 3.4, the proposed MMUE model may have more than one solution for UE link flow distribution as well as O-D travel cost. This non-uniqueness property renders existing transportation planning and design methods inapplicable. Traditionally, planners and designers evaluate a new design by assessing its unique UE solution. However, when there are alternative equilibrium flow distributions, it is more difficult to determine whether a design would achieve the specific goals. Among all the possible network equilibrium solutions, the one that minimizes the *TC* is referred to as the best-case solution, while the one that maximizes the *TC* is referred to as the worst-case solution. As an illustration, the best-case and worst-case solutions were respectively determined for the following two problems.

BC/WC-MMUE:

$$\min/\max_{(\boldsymbol{\beta},\boldsymbol{\chi},\boldsymbol{\lambda},\boldsymbol{\mu},\boldsymbol{\xi},\boldsymbol{\eta},\boldsymbol{\zeta},\boldsymbol{\psi},\boldsymbol{\omega},\boldsymbol{\alpha},\boldsymbol{f},\boldsymbol{h},\boldsymbol{v},\boldsymbol{\pi},\boldsymbol{e},\boldsymbol{d},\boldsymbol{\tau},\hat{\boldsymbol{\tau}},\boldsymbol{E})} \quad \Omega_1 \times TSTC + \Omega_2 \times TFC + \Omega_3 \times TEC$$

s.t. MMUE conditions (5)–(64), definitional constraints (89)–(93).

The above problems belong to the class of mathematical programs with complementarity constraints or MPCC, which is difficult to solve. Although many special algorithms have been developed to solve MPCCs (e.g., Luo et al., 1996; Fletcher and Leyffer, 2004; Lawphongpanich and Yin, 2010), only a few of them can be effectively applied to large-scale problems. In the present study, we

employed the algorithm proposed by Lawphongpanich and Yin (2010) using manifold sub-optimization. The algorithm enables convergence to a strongly stationary solution within a finite number of iterations. The detailed solution procedure is presented in Appendix C.

4.3. Model formulation

Because the MMUE problem has alternative solutions in terms of the aggregate link flow and O-D equilibrium total travel cost, the system performance associated with a plan for deploying charging lanes may also be non-unique. In practical applications, a design that optimizes the worst-case performance is more robust and preferred by planners, who tend to be risk-averse. For a given budget, the robust optimal deployment problem (RODP) of charging lanes for PHETs can be formulated as the following min-max program:

RODP:

$$\min_{\boldsymbol{y}} \max_{(\boldsymbol{\beta},\boldsymbol{\chi},\boldsymbol{\lambda},\boldsymbol{\mu},\boldsymbol{\xi},\boldsymbol{\eta},\boldsymbol{\zeta},\boldsymbol{\psi},\boldsymbol{\omega},\boldsymbol{\alpha},\boldsymbol{f},\boldsymbol{h},\boldsymbol{v},\boldsymbol{\pi},\boldsymbol{e},\boldsymbol{d},\boldsymbol{\tau},\hat{\boldsymbol{\tau}},\boldsymbol{E})} \Omega_1 \times TSTC + \Omega_2 \times TFC + \Omega_3 \times TEC$$

s.t. (5)–(64), (89)–(93)

$$\sum_{a\in\hat{L}(r)} y_a COB_a \le B \tag{94}$$

$$y_a \in \{0, 1\} \quad \forall\, a \in \hat{L}(r) \tag{95}$$

where COB_a denotes the cost of building charging lanes on link $a \in \hat{L}(r)$, and B is the budget.

The objective function is to minimize the maximum, or the worst-case system travel cost. Constraints (5)–(64) guarantee that the driver behavior follows the MMUE conditions. Constraints (89) and (90) specify the definitions of *TSTC* and *TFC*, and constraints (91)–(93) gives the expression of *TEC*. Constraint (94) is the budget constraint and constraint (95) ensures that the variable y_a is binary. It should be noted that, for a traffic network with MMUE, the system travel cost can be in time or monetary units depending on the primary concern of the system manager or planner (Yin and Yang, 2004). Although this paper only presents the money-based formulation, the time-based formulation is straightforward.

For convenience, let $\Theta(\boldsymbol{y})$ denote the feasible region of the inner problem, or the maximization part of the RODP; let θ denote the decision variable ($\boldsymbol{\beta}$, $\boldsymbol{\chi}$, $\boldsymbol{\lambda}$, $\boldsymbol{\mu}$, $\boldsymbol{\xi}$, $\boldsymbol{\eta}$, $\boldsymbol{\zeta}$, $\boldsymbol{\psi}$, $\boldsymbol{\omega}$, $\boldsymbol{\alpha}$, $\boldsymbol{f}$, $\boldsymbol{h}$, $\boldsymbol{v}$, $\boldsymbol{\pi}$, $\boldsymbol{e}$, $\boldsymbol{d}$, $\boldsymbol{\tau}$, $\hat{\boldsymbol{\tau}}$, $\boldsymbol{E}$); and let $\varsigma(\theta)$ denote the objective function. The inner problem can be expressed as

RODP-IN:

$$\varrho(\boldsymbol{y}) = \max_{\theta}\{\varsigma(\theta)\colon \theta \in \Theta(\boldsymbol{y})\}$$

Consequently, the RODP can be written as follows:

RODP-1:

$$\min_{\boldsymbol{y}} \varrho(\boldsymbol{y})$$

s.t.

$$\varrho(\boldsymbol{y}) = \max_{\theta}\{\varsigma(\theta)\colon \theta \in \Theta(\boldsymbol{y})\}$$

$$\sum_{a\in\hat{L}(r)} y_a COB_a \le B$$

$$y_a \in \{0, 1\} \quad \forall\, a \in \hat{L}(r)$$

Obviously, the feasible region of the inner problem is determined by the decision variables of the outer problem. A mathematical program with the above form is essentially a generalized semi-infinite min-max problem (see, e.g., Polak and Royset, 2005), which is not easy to solve. Moreover, owing to the MPCC property of the inner problem, existing algorithms (see, e.g., Still, 1999) may not be applicable to the RODP or RODP-1.

4.4. Solution algorithm

The heuristic algorithm proposed by Lou et al. (2010) was used to solve the RODP in this study. The basic idea of the algorithm is to use a differentiable penalty function to remove the constraints of the inner problem involving $\boldsymbol{y}$, thus transforming the RODP into an ordinary semi-infinite optimization problem. A cutting-plane scheme (e.g., Lawphongpanich and Hearn, 2004) is then used to solve a sequence of finite optimization problems, with each one better approximating the original problem than its predecessor.

In the inner problem, an auxiliary variable s_a is introduced to replace y_a. Consequently, constraints (19), (44), (25), (26), (27), (28) and (60), which involve y_a can be reformulated as follows:

$$E_j^{m,r} - E_i^{m,r} + e_a^{m,r} - s_a \hat{\tau}_a^{m,r} \varepsilon \le 0 \quad \forall\, (i,j) = a \in \hat{L}(r),\ r \in R_m^w,\ w \in W,\ m \in M1 \tag{96}$$

$$(E_j^{m,r}-E_i^{m,r}+e_a^{m,r}-s_a\hat{\tau}_a^{m,r}\varepsilon)\chi_{ij}^{m,r}=0 \quad \forall (i,j)=a\in\hat{L}(r), r\in R_m^w, w\in W, m\in M1 \tag{97}$$

$$s_aVOT^m-\lambda_a^{m,r}+\mu_a^{m,r}-\xi_a^{m,r}\geq 0 \quad \forall a\in\hat{L}(r), r\in R_m^w, w\in W, m\in M1 \tag{98}$$

$$(s_aVOT^m-\lambda_a^{m,r}+\mu_a^{m,r}-\xi_a^{m,r})\tau_a^{m,r}=0 \quad \forall a\in\hat{L}(r), r\in R_m^w, w\in W, m\in M1 \tag{99}$$

$$\lambda_a^{m,r}-s_a\varepsilon\chi_a^{m,r}\geq 0 \quad \forall a\in\hat{L}(r), r\in R_m^w, w\in W, m\in M1 \tag{100}$$

$$(\lambda_a^{m,r}-s_a\varepsilon\chi_a^{m,r})\hat{\tau}_a^{m,r}=0 \quad \forall a\in\hat{L}(r), r\in R_m^w, w\in W, m\in M1 \tag{101}$$

$$c_a^{m,r}=((1-s_a)t_a(v_a)+s_a\tau_a^{m,r})VOT^m+e_a^{m,r}VOE+d_a^{m,r}VOD \quad \forall a\in\hat{L}(r), r\in R_m^w, w\in W, m\in M1 \tag{102}$$

A penalized inner problem can thus be formulated as follows:

P-RODP-IN($\boldsymbol{y}$):

$$\max_{(\boldsymbol{\beta},\boldsymbol{\chi},\boldsymbol{\lambda},\boldsymbol{\mu},\boldsymbol{\xi},\boldsymbol{\eta},\boldsymbol{\zeta},\boldsymbol{\psi},\boldsymbol{\omega},\boldsymbol{\alpha},\boldsymbol{f},\boldsymbol{h},\boldsymbol{v},\boldsymbol{\pi},\boldsymbol{e},\boldsymbol{d},\boldsymbol{\tau},\hat{\boldsymbol{\tau}},\boldsymbol{E})} \Omega_1\times TSTC+\Omega_2\times TFC+\Omega_3\times TEC-K_2\sum_{w\in W}(s_a-y_a)^2$$

s.t. (1)–(18), (20)–(24), (29)–(43), (45)–(59), (61)–(64), (89)–(93), (96)–(102)

where K_2 is a sufficiently large constant.

For convenience, let Ξ denote the feasible region of P-RODP-IN($\boldsymbol{y}$), and $\hat{\varsigma}(\theta,\boldsymbol{s},\boldsymbol{y})$ the objective function. For a finite penalty, the optimal objective function value of P-RODP-IN($\boldsymbol{y}$) is an upper bound of the original inner problem. For a given $\boldsymbol{y}$, let $\bar{\theta}$ denote the optimal solution of the original inner problem RODP-IN, let $(\bar{\theta},\bar{\boldsymbol{s}})$ represent the optimal solution of the above P-RODP-IN($\boldsymbol{y}$) with fixed $\theta=\bar{\theta}$, and let $(\hat{\theta},\hat{\boldsymbol{s}})$ solve the above panelized problem for some $K_2>0$. We thus have $\varsigma(\bar{\theta})=\hat{\varsigma}(\bar{\theta},\bar{\boldsymbol{s}},\boldsymbol{y})\leq\hat{\varsigma}(\hat{\theta},\hat{\boldsymbol{s}},\boldsymbol{y})$. The first equality is based on that, if $\theta=\bar{\theta}$, $\bar{\boldsymbol{s}}$ maximizes P-RODP-IN($\boldsymbol{y}$) when involving no penalty, i.e., when $\bar{\boldsymbol{s}}=\boldsymbol{y}$. The second inequality is based on $(\bar{\theta},\bar{\boldsymbol{s}})$ being a feasible solution for the penalized problem. When K_2 approaches infinite, P-RODP-IN($\boldsymbol{y}$) tends to be equivalent to the original inner problem.

A penalized version of the robust optimal deployment problem RODP can be formulated as follows:

P-RODP:

$$\min_{\boldsymbol{y}}\max_{\theta,\boldsymbol{s}}\hat{\varsigma}(\theta,\boldsymbol{s},\boldsymbol{y})$$

s.t.

$$(\theta,\boldsymbol{s})\in\Xi$$

$$\sum_{a\in\hat{L}(r)}y_aCOB_a\leq B$$

$$y_a\in\{0,1\} \quad \forall a\in\hat{L}(r)$$

The objective of P-RODP is to minimize the upper bound of the total system travel cost. When the penalty parameter K_2 is sufficiently large, the upper bound will be quite tight and the solution of P-RODP may also minimize the worst-case system travel cost. Moreover, P-RODP is an ordinary semi-infinite min–max problem because its inner problem is defined on a feasible region that is independent of the decision variables of the outer problem. By introducing an auxiliary variable σ, P-RODP can be equivalently reformulated as follows:

P-RODP-1:

$$\min_{\boldsymbol{y},\sigma}\sigma$$

s.t.

$$\sigma\geq\hat{\varsigma}(\theta,\boldsymbol{s},\boldsymbol{y}) \quad \forall (\theta,\boldsymbol{s})\in\Xi$$

$$\sum_{a\in\hat{L}(r)}y_aCOB_a\leq B$$

$$y_a\in\{0,1\} \quad \forall a\in\hat{L}(r)$$

P-RODP-1 can be solved using a cutting-plane scheme. Assuming that $(\theta^1,\boldsymbol{s}^1)$, $(\theta^2,\boldsymbol{s}^2)$, $\cdots$,$(\theta^n,\boldsymbol{s}^n)$ are elements of Ξ, a relaxed version of P-RODP-1 can be obtained as follows:

R-P-RODP-1:

$$\min_{\boldsymbol{y},\sigma}\sigma$$

s.t.

$$\sigma\geq\hat{\varsigma}(\theta^i,\boldsymbol{s}^i,\boldsymbol{y}) \quad \forall i=1,2,\cdots,n$$

$$\sum_{a \in \hat{L}(r)} y_a COB_a \le B$$

$$y_a \in \{0, 1\} \quad \forall\, a \in \hat{L}(r)$$

Obviously, in the above R-P-RODP-1 problem, a discrete subset $\bar{\Xi} = \{(\theta^1, \boldsymbol{s}^1), (\theta^2, \boldsymbol{s}^2), \cdots, (\theta^n, \boldsymbol{s}^n)\}$ is used to approximate the set Ξ in the original P-RODP-1 problem. If a global optimal solution of R-P-RODP-1 denoted by $(\tilde{\boldsymbol{y}}, \tilde{\sigma})$ is feasible for the original P-RODP-1 problem, it would be an optimal solution of P-RODP-1. The feasibility can be assessed by solving problem P-RODP-IN($\tilde{\boldsymbol{y}}$) and comparing its optimal value $\hat{\varsigma}(\tilde{\theta}, \tilde{\boldsymbol{s}}, \tilde{\boldsymbol{y}})$ with σ. If $\hat{\varsigma}(\tilde{\theta}, \tilde{\boldsymbol{s}}, \tilde{\boldsymbol{y}}) \le \tilde{\sigma}$, then $(\tilde{\boldsymbol{y}}, \tilde{\sigma})$ is a feasible and optimal solution of P-RODP-1. However, if $\hat{\varsigma}(\tilde{\theta}, \tilde{\boldsymbol{s}}, \tilde{\boldsymbol{y}}) > \tilde{\sigma}$, $(\tilde{\boldsymbol{y}}, \tilde{\sigma})$ is infeasible for P-RODP-1, in which case $(\tilde{\theta}, \tilde{\boldsymbol{s}})$ is added to the discrete set $\bar{\Xi}$ and R-P-RODP-1 is solved again to obtain an improved solution.

The solution procedure outlined above can be summarized as follows:

Step 0: Solve WC-MMUE with an initial deployment plan $\boldsymbol{y}^0$ to obtain an initial solution θ^1. Set $k = 1$, $\boldsymbol{s}^1 = \boldsymbol{y}^0$, and $\bar{\Xi}^1 = \{(\theta^1, \boldsymbol{s}^1)\}$.
Step 1: Let $(\boldsymbol{y}^k, \sigma^k)$ solve R-P-RODP-1 over the discrete set $\bar{\Xi}^k$.
Step 2: Let $(\theta^{(k+1)}, \boldsymbol{s}^{(k+1)})$ solve P-RODP-IN($\boldsymbol{y}^k$).
Step 3: If $\hat{\varsigma}(\theta^{(k+1)}, \boldsymbol{s}^{(k+1)}, \boldsymbol{y}^k) \le \sigma^k$, stop and $\boldsymbol{y}^k$ is a robust optimal deployment plan. Otherwise, set $\bar{\Xi}^{(k+1)} = \bar{\Xi}^k \cup \{(\theta^{(k+1)}, \boldsymbol{s}^{(k+1)})\}$ and $k = k + 1$ and go back to Step 1.

It should be noted that P-RODP-IN($\boldsymbol{y}$) is also an MPCC and can be solved using a procedure similar to that in Appendix C.

5. Numerical studies

In this section, three numerical examples are presented to demonstrate the proposed models.

5.1. Scenario 1: Three-node toy network

Consider a toy network with three nodes, four links, three O-D pairs (1,2), (1,3) and (2,3), as shown in Fig. 2. It is assumed that all four links are candidate charging links. The relevant parameters are as follows:

(a) User class set: $M1 = \{1\}$, $M2 = \{2\}$, where classes 1 and 2 are PHET users and passenger car users, respectively.
(b) Demand: $q_1^{12} = 10$, $q_2^{12} = 0$, $q_1^{13} = 15$, $q_2^{13} = 0$, $q_1^{23} = 5$, $q_2^{23} = 50$,
(c) PCE conversion factors: $\gamma^1 = 2.0$, $\gamma^2 = 1.0$
(d) Link performance function: $t_1(v_1) = 40 + v_1$, $t_2(v_2) = 5 + v_2$, $t_3(v_3) = 15 + v_3$, $t_4(v_4) = 10 + 0.5v_4$
(e) Energy consumption: $\varpi_1^1 = 600$, $\varpi_2^1 = 300$, $\varpi_3^1 = 300$, $\varpi_4^1 = 300$
(f) Energy efficiency: $TWE^1 = 4$, $TWD^1 = 1$
(g) Unit energy cost: $VOE = 1$, $VOD = 1$
(h) Value of time: $VOT^1 = 2$, $VOT^2 = 1$
(i) Battery parameter: $E_{max}^1 = 50$, $b_{up}^1 = 1$, $b_{lo}^1 = 0$, $E_0^1 = 50$
(j) Charging rate on charging link: $\varepsilon = 1$
(k) Costs of deploying charging links: $COB_1 = 800$, $COB_2 = 100$, $COB_3 = 200$, $COB_4 = 400$

Let both emission index EI_l and external cost factor ϱ_l equal 0.1 for all four pollutants, and the heat content of diesel ϑ equal 1. Let weighting parameter Ω_1, Ω_2, and Ω_3 all equal 1. Note that the values of parameters in the toy network are only for illustration purpose. More realistic value of the parameters will be provided in the following scenarios 2 and 3. Four different budget levels, i.e., $B = 100,\ 300,\ 700,\ 1500$, are respectively investigated.

By implementing the proposed model in the toy network, robust optimal deployment plans corresponding to the different budget levels were obtained. The results are presented in Table 2, where the zero budget level is also listed as a reference of the status quo (i.e., no charging lanes). Through enumerating all 16 combinations of deployed charging links and comparing their worst-case system performance, we verified that the solutions listed in Table 2 are indeed the robust optimal solutions. It can be observed from Table 2

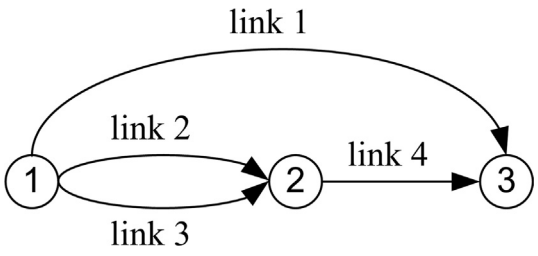

Fig. 2. A network with three nodes.

Table 2
Robust optimal deployment of charging lanes on the toy network.

Budget	Deployed Charging Lanes	Best-case *TC*	Worst-case *TC*	Worst-case improvement versus the status quo
0	–	14,025	14,025	–
100	Link 2	13,171	13,171	6.09%
300	Links 2 and 3	12,595	12,795	8.77%
700	Links 2, 3 and 4	10,175	10,375	26.02%
1500	Links 1, 2 and 3	9655	9655	31.16%

that, for the first three budget levels, i.e., $B = 100,\ 300$, or 700, the model converts all links, whose total cost are within the budgets, into charging links; and with the increase of budget, more links are converted into charging links and the worst-case system *TC* becomes lower. However, for the last budget level, i.e., $B = 1500$, which is enough to convert all four links into charging links, only links 1, 2 and 3 are chosen for conversion into charging links. It can also be observed that, the best-case *TC* and worst-case *TC* are identical for budget level of 0, 100 and 1500, while they are different for budget level of 300 and 700.

To show the importance of considering the non-uniqueness property of the network equilibrium model and the benefits of employing a robust optimization framework, we provide an interesting comparison in Table 3. As shown in Table 3, deployment plan 1 is the robust optimal solution under the budget level of 1500, and plan 2 is another feasible solution that converts all four links into charging links. It can be observed from Table 3 that although the best-case performance of plan 1 is slightly worse than plan 2, the worst-case performance of plan 1 is much better than plan 2. The plan 1 is thus more robust than plan 2. If the non-uniqueness of the network equilibrium pattern is ignored and the charging lanes are deployed without considering the worst-case situation, a sub-optimal or even inferior deployment plan (e.g., plan 2) might be implemented.

5.2. Scenario 2: Nguyen-Dupuis network

The Nguyen-Dupuis network (see Fig. 3) consists of 13 nodes, 19 links, and four O-D pairs. The link travel time function is assumed to be $t_a(v_a) = b_a^0 + b_a^1 v_a$ min, where b_a^0 and b_a^1 are predetermined parameters. Table A.1 (see Appendix A) reports the parameters b_a^0, b_a^1 and the length of each link. Two user classes are considered, $M1 = \{1\}$, $M2 = \{2\}$, where classes 1 and 2 are PHET users and passenger car users, respectively. The travel demand of class 2 passenger cars is given by (Nguyen and Dupuis, 1984): $q_2^{12} = 400veh/h$; $q_2^{13} = 800veh/h$; $q_2^{42} = 600veh/h$; $q_2^{43} = 200veh/h$. Assume that for each O-D pair, the travel demand of class 1 PHETs is one-tenth of passenger cars. For simplicity, we assume a constant energy consumption rate of 3 kWh/mi for PHETs, and the energy consumption on a link is simply the product of its length and the energy consumption rate. The cost of converting a link into a charging link is assumed to be one unit cost per mile and the budget B is 100 units. Let weighting parameter Ω_1, Ω_2, and Ω_3 all equal 1. The emission index EI_l and external cost factor φ_l are listed in Table 4. EI_l is calculated based on the emission standards for heavy-duty engines (USEPA, 2007) and φ_l is provided by Matthews (1999). All other predetermined parameters in our model are summarized in Table 5. The values of VOT^1 and VOT^2 are provided by Ayala (2014). Fuel efficiencies TWE^1 and TWD^1 are based on the data in USDOE (2017a,2017b). Fuel prices *VOE* and *VOD* are from Alternative Fuels Data Center, (2017). Note that the value of *VOD* is calculated based on that the price of diesel is \$2.48/gallon and the heat content of diesel is 35 kWh/gallon (Alternative Fuels Data Center, 2014). The conversion factor into PCE for class 1 PHET, i.e., γ^1 is from the Highway Capacity Manual (HCM) 6th edition (TRB, 2010). Note that the network is assumed to be in level terrain. The values of K_1 and K_2 are based on preliminary results. The proposed algorithm is implemented using GAMS (Rosenthal, 2012).

From our GAMS implementation on a 3.40 GHz Dell Computer with 16 GB of RAM, we obtain a deployment plan that locates charging lanes on links (5,6), (6,10), and (10,11). Compared with the status quo condition (i.e., no charging lanes), the optimal design reduces the worst-case system total cost *TC* from 117772.12 to 106521.65, a reduction of 9.55 percent. More specifically, the deployed charging links do not change the *TSTC*, reduce the *TFC* from 31943.25 to 21655.61, and decrease the *TEC* from 1468.58 to 505.75.

Table 6 illustrates the impacts of deployed charging lanes on different user groups. It can be observed that, for all four O-D pairs, the deployed charging links do not change the O-D travel cost of passenger cars but cut down the equilibrium O-D travel cost of PHETs by nearly 25 percent. Through further comparison of the link flow and path flow solutions between the status quo condition and the optimal deployment plan, we obtained several interesting observations. First, for the status quo condition and the optimal deployment plan, the aggregate link flow solutions are identical and unique in this example. Second, in the status quo condition, each O-D pair has alternative path flow solutions for both passenger cars and PHETs, while in the optimal deployment plan, the path flow solutions for PHETs become unique. Third, the path flow solutions for the optimal deployment plan are also one of the path flow

Table 3
Comparison between two deployment plans with sufficient budget.

Plan Number	Deployed Charging Lanes	Best-case *TC*	Worst-case *TC*
1	Links 1, 2 and 3	9655	9655
2	Links 1, 2, 3 and 4	9275	10,375

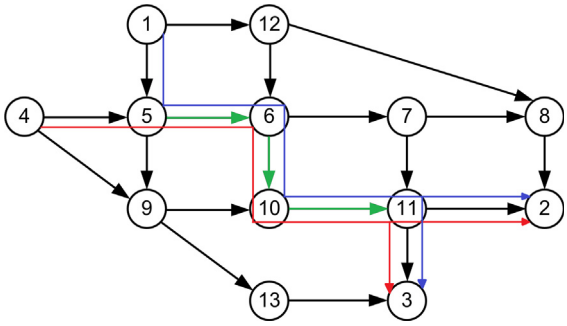

Fig. 3. Nguyen-Dupuis network.

Table 4
Emission parameters.

	CO	HC	NO_x	PM
EI_l (g/gallon)	203.44	1.84	2.63	0.13
ϱ_l ($/g)	0.54×10^{-3}	1.42×10^{-3}	1.06×10^{-3}	2.82×10^{-3}

Table 5
Parameter values for Scenario 2.

Notation	Description	Value
VOT^1	Value of time for class 1 PHET drivers ($/h)	20.3
VOT^2	Value of time for class 2 passenger car drivers ($/h)	15.7
TWE^1	Tank-to-wheel efficiency of electricity for class 1 PHET	0.70
TWD^1	Tank-to-wheel efficiency of diesel for class 1 PHET	0.19
VOE	Value of one unit of electricity ($/kWh)	0.13
VOD	Value of one unit of diesel ($/kWh)	0.07
γ^1	Conversion factor into PCE for class 1 PHETs	2.0
γ^2	Conversion factor into PCE for class 2 passenger cars	1.0
E^1_{max}	Battery size for class 1 PHET (kWh)	30
b^1_{lo}	The coefficient that sets the lower bound of battery level	20%
b^1_{up}	The coefficient that sets the upper bound of battery level	90%
E^1_0	Initial battery level (kWh)	27
$\tilde{t}_a$	The maximum allowable travel time on link a (min)	10,000
ε	Recharging rate of PHETs on charging lanes (kW)	300
K_1	A large constant value	10,000
K_2	A large constant value	10,000

solutions for the status quo condition. Because the deployed charging links do not change the aggregate link flow distribution, the minimum travel time specified by the link performance function will not change, and then the equilibrium O-D travel cost for passenger cars will remain unchanged. As shown in Fig. 3, the green links (5,6), (6,10) and (10,11) are deployed charging links, the blue lines depict the utilized paths by PHETs between O-D pair (1,2) and (1,3), and the red lines depict the utilized paths by PHETs between O-D pairs (4,2) and (4,3). It can be observed that all four paths pass through the three deployed charging links. Although the deployed charging links attract all PHETs of the four O-D pairs to use them, passenger cars that originally pass through these links can switch to other alternative paths to maintain their minimum O-D travel cost.

Table 6
O-D travel cost comparison between status quo and optimal design for the Nguyen-Dupuis network.

OD	Status quo OD cost		Optimal design OD cost		Percentage change (%)	
	Passenger cars	PHETs	Passenger cars	PHETs	Passenger cars	PHETs
(1, 2)	143.52	208.23	143.52	156.79	0	-24.7
(1, 3)	145.00	208.73	145.00	157.29	0	-24.6
(4, 2)	139.36	206.82	139.36	155.38	0	-24.9
(4, 3)	140.84	207.32	140.84	155.88	0	-24.8

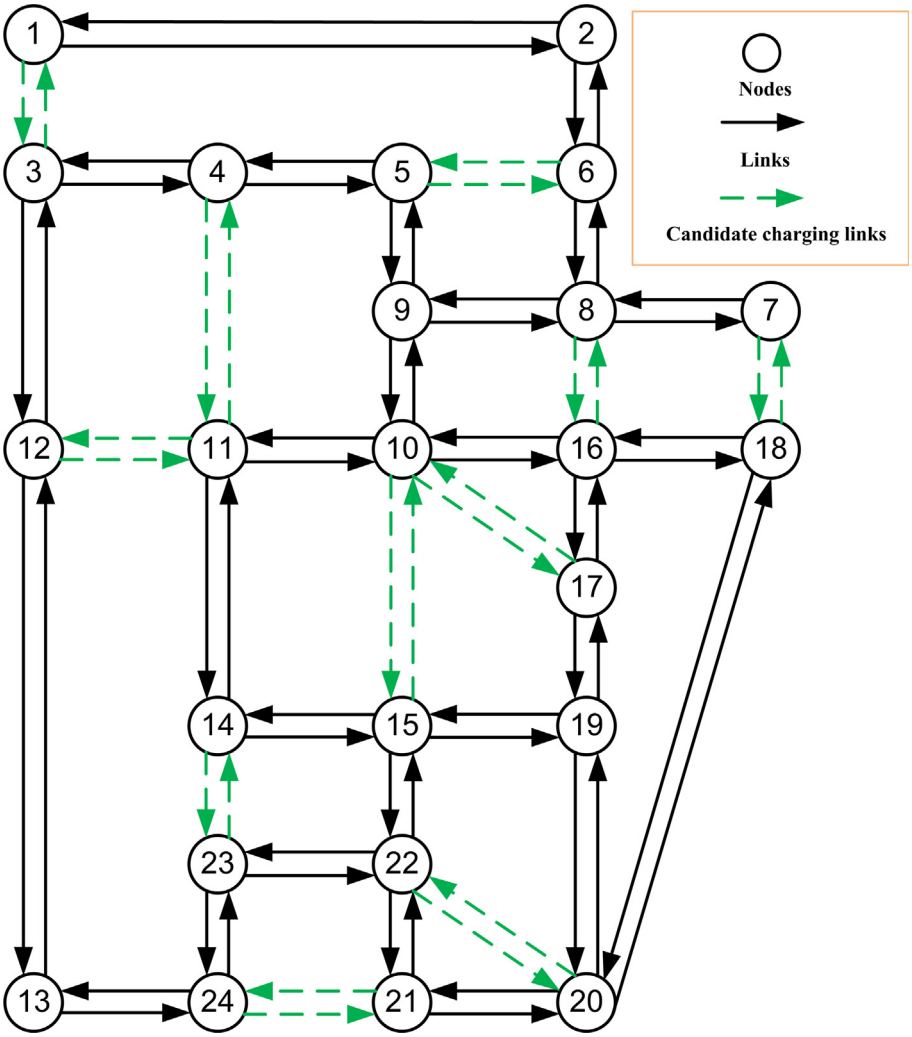

Fig. 4. Sioux Falls network.

The results of this example suggest that it is possible for strategically deployed charging lanes to benefit PHET users while having no adverse effect on other users.

5.3. Scenario 3: Sioux Falls network

To further test the proposed model, we solve it for the Sioux Falls network, which consists of 24 nodes, 76 links, as shown in Fig. 4. Because the original Sioux Falls network mainly consists of urban arterials, to better illustrate our model, we maintain the topology of the network and utilize a set of revised link characteristics, which is provided by Chen et al. (2016), to represent a regional freeway network that connects logistic centers. Particularly, we adopt the Bureau of Public Roads (BPR) function as the link performance functions. Two user classes are considered, $M1 = \{1\}$, $M2 = \{2\}$, where classes 1 and 2 are PHET users and passenger car users, respectively. The O-D demands of class 2 passenger cars are given in Table A.2, and the class 1 PHET demands are assumed to be one-fifth of passenger car demands. In the base case, the cost of converting a link into a charging link is assumed to be one thousandth of the product of its length and capacity. As shown in Fig. 4, the network has 22 candidate charging links. The budget is set as 750 units. All other parameters are the same as those in scenario 2.

The model provides a deployment plan that locates charging lanes on links (1,3), (5,6), (6,5), (21,24), and (24,21). Compared with the status quo condition (i.e., no charging lanes), the plan reduces the *TC* from 2,619,457 to 2,508,682, a reduction of 4.2%. To be specific, the charging links reduce the *TFC* from 906,422 to 809,600, a reduction of 10.7%, decrease the *TEC* from 38,962 to 29,751, a decrease of 23.6%, and reduce the *TSTC* from 1,674,073 to 1,669,331, a reduction of 0.3%. The reduction in *TFC* and *TEC* is the direct benefits from charging link deployment because charging links can supply PHETs with electric power and thus reduce fuel and emission costs. The slight reduction in *TSTC* demonstrates a potential indirect benefit of charging links. Strategically deployed charging links may be able to attract PHETs away from congested roads and thus reduce system congestion. Although the deployed

Table 7
O-D travel cost comparison between status quo and optimal design for the Sioux Falls network.

OD	Status quo OD cost		Optimal design OD cost		Percentage change (%)	
	Passenger cars	PHETs	Passenger cars	PHETs	Passenger cars	PHETs
(1, 2)	4.87	11.99	4.42	11.41	−9.3	−4.9
(2, 13)	12.41	68.05	12.44	56.95	0.3	−16.3
(4, 5)	1.5	7.63	1.5	7.63	0	0
(4, 7)	9.20	55.48	9.08	45.83	−1.3	−17.4
(5, 21)	14.82	93.99	14.82	84.62	0	−10.0
(7, 20)	8.07	32.97	7.32	32.00	−9.3	−2.9
(13, 4)	6.44	42.09	6.44	42.09	0	0
(20, 18)	6.40	22.39	6.59	22.63	2.9	1.1
(24, 13)	6.06	21.94	5.94	21.79	−1.9	−0.7
(24, 21)	4.30	15.46	4.33	11.92	0.8	–22.9

charging links can improve the system performance, they may not benefit all travelers. Table 7 reports the change of equilibrium O-D travel cost of 10 representative O-D pairs for passenger cars and PHETs. It can be observed that the deployed charging links may benefit or have no influence on some users, while making certain users worse off slightly. It is an important direction for future studies to take the equity among different user groups into consideration.

In order to investigate the impact of the charging lane cost on the deployment solution, we further solve the proposed model for five different charging lane cost, i.e., 4.0, 2.0, 0.5, 0.25, and 0.125 times of the cost in the base case while the values for other parameters remain unchanged. The resulting solutions for system performance are shown in Fig. 5. It is shown from Fig. 5 that, when the charging lane cost is higher than 0.25 times of the cost in the base case, system total cost (*TC*), total fuel cost (*TFC*) and total emission cost (*TEC*) decrease with a decrease in the charging lane cost, while the change of total system travel time cost (*TSTC*) has no obvious trend. This result is expected because: (1) with given budget more charging lanes can be deployed with a decrease of charging lane cost, the overall system performance can thus be further improved; (2) the major benefit of charging lanes is to reduce fuel cost and exhaust emissions, therefore, with more strategically deployed charging lanes *TFC* and *TEC* can be reduced; (3) due to the fact that charging lanes are converted from regular lanes and will not have increased traffic capacity and that PHETs may slow down to improve their recharging time on charging lanes, *TSTC* may not always be reduced with more charging lanes. Fig. 5 also shows that when the charging lane cost further decrease from 0.25 times to 0.125 times of the cost in the base case, the system performance does not change. This result is also reasonable because when all beneficial candidate charging lanes have been affordable, further cost reduction will not lead to more improvement in system performance.

6. Conclusions

In this study, we investigated the strategic development of an electrified road freight transportation system that utilizes dynamic charging technology and plug-in hybrid electric trucks. A series of mathematical models were developed to determine the optimal

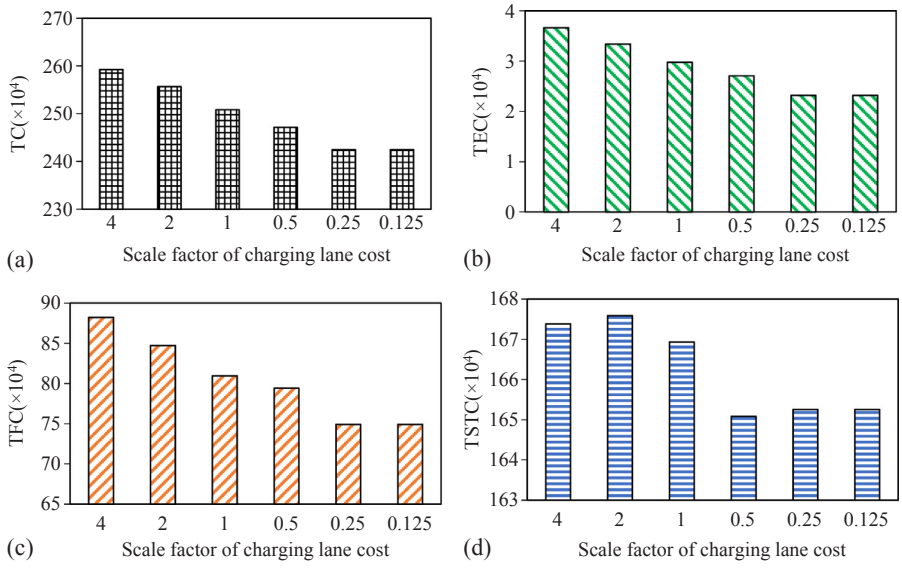

Fig. 5. System performance with different charging lane cost. (a) *TC* (b) *TEC* (c) *TFC* (d) *TSTC*.

deployment of the dynamic charging lanes for PHETs in a general road network. PHET drivers were assumed to attempt to minimize their generalized travel cost, which is determined by the travel time and fuel cost, while other drivers were assumed to only consider travel time. For a given route connecting a PHET driver's origin and destination, a linear program was formulated to describe the driver's decision on whether to use electricity or fossil fuel, and on the use of the charging lanes. A network equilibrium model was then formulated as a VI problem and an algorithm for the efficient solution of the problem was developed. It was found that the equilibrium model might have non-unique flow distributions and equilibrium O-D travel cost. An MPCC problem was thus formulated to determine the best- and worst-case network equilibrium patterns and a manifold sub-optimization algorithm was used to solve it. Based on the network equilibrium conditions and taking the non-uniqueness of the equilibrium patterns into consideration, we developed a robust optimal deployment model for determining the network links to be converted into charging lanes on a limited budget. As formulated, the proposed model represents a generalized semi-infinite min-max problem, which is not easy to solve. An iterative heuristic algorithm was used for its solution in the present study. A three-node toy network and the Sioux Falls network were used for the numerical demonstration of the proposed charging lane deployment model. The results show that, charging lanes can significantly reduce the diesel consumption and pollutant emissions from PHETs, and that the robust optimization model can guard against the worst-case scenario.

Future research work will be undertaken in several aspects. First, one limitation of this study is that the solution existence of the proposed network equilibrium model is not discussed. We leave the work of investigating the solution existence of the network equilibrium model for future studies. Second, the network equilibrium model can be extended by considering the potential influence of charging lanes on the driving behaviors of electric vehicles other than PHETs. For instance, the behaviors of battery electric vehicles with range limits can be captured using the UE model proposed by Chen et al. (2016). Third, the network equilibrium model can be improved by considering flow-dependent or speed-dependent energy consumption (see e.g., He et al., 2014; Xu et al., 2017; Liu and Song, 2018 for UE of BEVs considering flow-dependent electricity consumption). Fourth, the charging lane deployment model can be extended by considering risk-neutral and risk-acceptant preferences of planners. Fifth, further study is planned to consider the equality of different user groups when employing the proposed model. In other words, to ensure that the dynamic charging lanes are deployed such that most PHETs are better off while other users are not worse off, implying a Pareto-improving design (Song et al., 2009, 2014; Lawphongpanich and Yin, 2010; and Guo and Yang, 2010). In addition, the development of even more efficient algorithms for solving the proposed model will also be undertaken.

Acknowledgment

The study was partially sponsored by Mountain-Plains Consortium, a regional University Transportation Center sponsored by the U.S. Department of Transportation, and the U.S. Department of Energy (DE-EE0007997, DE-AR0000885). The views expressed are those of the authors and do not reflect the official policy or position of the project's sponsors.

Appendix A. Notations and tables.

Notations

Sets	**Description**
N	Set of nodes
A	Set of links
W	Set of O-D pairs
M	Set of user classes
$M1$	Set of all classes of PHET users
$M2$	Set of all classes of users that use vehicles that are not PHETs
$\hat{L}$	Set of candidate charging links
L	Set of links that are not considered for deploying charging links
R_m^w	Set of routes for O-D pair w, class m
$N(r)$	Set of nodes of route $r \in R_m^w$ for O-D pair $w \in W$, class $m \in M$
$A(r)$	Set of links of route $r \in R_m^w$ for O-D pair $w \in W$, class $m \in M$
$\hat{L}(r)$	Set of candidate charging links of route $r \in R_m^w$ for O-D pair $w \in W$, class $m \in M$
$L(r)$	Set of links that are not considered for deploying charging links along route $r \in R_m^w$
Parameters	**Description**
$i,\ j,\ k$	Subscript for nodes, $i \in N,\ j \in N,\ k \in N$
a	Subscript for links, $a = (i, j) \in A$
w	Subscript for O-D pairs, $w \in W$
m	Subscript for user classes, $m \in M$
r	Subscript for routes, $r \in R_m^w$
δ_a^r	Route-link incidence
q_m^w	Travel demand for O-D pair $w \in W$, class $m \in M$

$O(w)$, $D(w)$	Origin and destination nodes of O-D pair $w \in W$
$\tilde{t}_a$	Maximum allowable travel time on link a
γ^m	Conversion factor into PCE for the total link flow of class $m \in M$
E^m_{max}	Battery size for class $m \in M1$ PHETs
b^m_{lo}, b^m_{up}	The coefficient that sets the lower bound and upper bound of battery level
E^m_0	Initial battery level for class $m \in M1$ PHETs
ϖ^m_a	Total energy consumption of class $m \in M1$ PHETs on link a
ε	Recharging rate on charging lanes
VOT^m	Value of time for class $m \in M$ users
TWE^m, TWD^m	Tank-to-wheel efficiency of electric motor and diesel engine for class $m \in M1$ PHETs, respectively
VOE, VOD	Value of one unit of electricity and diesel, respectively
COB_a	Cost of building charging lanes on link $a \in \hat{L}(r)$
B	Budget
K^1, K^2	Two sufficiently large constants

Variables	**Description**
y_a	A binary variable indicating whether to deploy charging lanes on link $a \in \hat{L}$.
f^m_r	Traffic flow of class $m \in M$ on route $r \in R^w_m$
h^m_a	Total link flow of class $m \in M$ on link $a \in A$
v_a	Total link flow in passenger car equivalence (PCE)
$t_a(v_a)$	Travel time on link $a \in A$ specified by the link performance function
$\tau^{m,r}_a$	Actual travel time that class $m \in M1$ PHETs spend on link a along a route$r$
$\hat{\tau}^{m,r}_a$	Recharging time of class $m \in M1$ PHETs on link a along route$r$
$c^{m,r}_a$	Generalized travel cost of class $m \in M1$ PHETs on link $a \in A$ along route$r$
$E^{m,r}_i$	Battery level of class $m \in M1$ PHETs at node $i \in N(r)$ along route$r$
$e^{m,r}_a$	Electricity consumption of class $m \in M1$ PHETs on link $a \in A$ along route$r$
$d^{m,r}_a$	Diesel consumption of class $m \in M1$ PHETs on link $a \in A$ along route$r$
π^w_m	Equilibrium travel cost for class $m \in M$ users between O-D pair $w \in W$.

See Tables A.1 and A.2.

Table A.1
Link characteristics of the Nguyen- Dupuis network.

Link	b^0_a (min)	b^1_a	Length (mi)	Link	b^0_a (min)	b^1_a	Length (mi)
1–5	25	0.0075	29.17	8–2	25	0.0125	29.17
1–12	25	0.01	29.17	9–10	25	0.005	29.17
4–5	25	0.01	29.17	9–13	55	0.005	58.34
4–9	50	0.005	58.34	10–11	25	0.0025	29.17
5–6	25	0.0025	29.17	11–2	25	0.005	29.17
5–9	25	0.0075	29.17	11–3	25	0.0075	29.17
6–7	25	0.01	29.17	12–6	25	0.0025	29.17
6–10	25	0.005	29.17	12–8	80	0.01	87.51
7–8	25	0.0125	29.17	13–3	25	0.01	29.17
7–11	25	0.0125	29.17				

Table A.2
O-D demand of passenger cars in the Sioux Falls network.

O\D	1	2	4	5	7	13	18	20	21	24
1	0	500	2500	1000	2500	2500	500	1500	500	500
2	500	0	1000	500	1000	1500	1000	500	1000	1000
4	2500	1000	0	2500	200	3000	500	1500	1000	1000
5	1000	500	2500	0	1000	1000	1000	500	500	1000
7	2500	1000	2000	1000	0	2000	1000	2500	1000	500
13	2500	1500	3000	1000	2000	0	500	3000	3000	4000
18	500	1000	500	1000	1000	500	0	2000	500	1000
20	1500	500	1500	500	2500	3000	2000	0	6000	2000
21	500	1000	1000	500	1000	3000	500	6000	0	2500
24	500	1000	1000	1000	500	3500	1000	2000	2500	0

Appendix B. Proof of the equivalence between the optimal objective function value of P1 and P2

First of all, because P1 and P2 have identical objective function and the feasible region of P1 is a subset of the feasible region of P2, the optimal objective function value of P1 is no better than that of P2. Then if we can further prove that the optimal objective function value of P2 is no better than that of P1, P1 and P2 must have identical optimal objective function value.

Let $e_a^{m,r*}$, $d_a^{m,r*}$, $\tau_a^{m,r*}$, $\hat{\tau}_a^{m,r*}$ and $E_i^{m,r*}$ denote the optimal solution of P2. First, for P2, constraint (17) must be binding in the optimal solution, i.e., $e_a^{m,r*}$ and $d_a^{m,r*}$ satisfy constraint (1), otherwise fuel cost in the objective function can further be reduced. We then aims to prove that we can find $\hat{\tau}_a^{m,r\dagger}$ and $E_i^{m,r\dagger}$ such that $e_a^{m,r*}$, $d_a^{m,r*}$, $\tau_a^{m,r*}$, $\hat{\tau}_a^{m,r\dagger}$ and $E_i^{m,r\dagger}$ is a feasible solution of P1. Based on this and considering the fact that P1 and P2 have identical objective function that only involves $e_a^{m,r}$, $d_a^{m,r}$ and $\tau_a^{m,r}$, the optimal objective function value of P2, which is determined by $e_a^{m,r*}$, $d_a^{m,r*}$ and $\tau_a^{m,r*}$, must be no better than that of P1 because a feasible solution to P1 should be no better than its optimal solution.

We define $\hat{\tau}_a^{m,r\dagger}$ and $E_i^{m,r\dagger}$ with the following equations:

$$E_{O(w)}^{m,r\dagger} = E_0^m$$

$$E_j^{m,r\dagger} = E_i^{m,r\dagger} - e_a^{m,r*},\ \forall\ (i,j) = a \in L(r)$$

$$E_j^{m,r\dagger} = \min\{E_i^{m,r\dagger} - e_a^{m,r*} + y_a\tau_a^{m,r*}\varepsilon,\ E_{max}^m b_{up}^m\},\ \forall\ (i,j) = a \in \hat{L}(r)$$

$$\hat{\tau}_a^{m,r\dagger} = \frac{E_j^{m,r\dagger} - E_i^{m,r\dagger} + e_a^{m,r*}}{y_a\varepsilon},\ \forall\ (i,j) = a \in \hat{L}(r)$$

(a) It is easy to see that $e_a^{m,r*}$, $\hat{\tau}_a^{m,r\dagger}$ and $E_i^{m,r\dagger}$ satisfy equality constraints (2)–(4)

(b) We prove that $E_i^{m,r\dagger}$ satisfies constraint (5), i.e., $E_i^{m,r\dagger} \leqslant E_{max}^m b_{up}^m,\ \forall\ i \in N(r)$. We first prove that for any $(i,j) = a \in A(r)$, if $E_i^{m,r\dagger} \leqslant E_{max}^m b_{up}^m$, we will always have $E_j^{m,r\dagger} \leqslant E_{max}^m b_{up}^m$. First, if $(i,j) = a \in L(r)$, $E_j^{m,r\dagger} = E_i^{m,r\dagger} - e_a^{m,r*}$, from constraint (14) we have $E_j^{m,r\dagger} = E_i^{m,r\dagger} - e_a^{m,r*} \leqslant E_i^{m,r\dagger} \leqslant E_{max}^m b_{up}^m$. Second, if $(i,j) = a \in \hat{L}(r)$, $E_j^{m,r\dagger} = \min\{E_i^{m,r\dagger} - e_a^{m,r*} + y_a\tau_a^{m,r*}\varepsilon,\ E_{max}^m b_{up}^m\} \leqslant E_{max}^m b_{up}^m$. Therefore, based on $E_{O(w)}^{m,r\dagger} = E_0^m \leqslant E_{max}^m b_{up}^m$, we will always have $E_i^{m,r\dagger} \leqslant E_{max}^m b_{up}^m,\ \forall\ i \in N(r)$.

(c) We prove that $E_i^{m,r\dagger}$ satisfies constraint (6), i.e., $E_i^{m,r\dagger} \geqslant E_{max}^m b_{lo}^m,\ \forall\ i \in N(r)$. We first prove that for any $(i,j) = a \in A(r)$, if $E_i^{m,r\dagger} \geqslant E_i^{m,r*}$, we will always have $E_j^{m,r\dagger} \geqslant E_j^{m,r*}$. First, if $(i,j) = a \in L(r)$, $E_j^{m,r\dagger} = E_i^{m,r\dagger} - e_a^{m,r*} \geqslant E_i^{m,r*} - e_a^{m,r*}$, from constraint (18) we have $E_j^{m,r\dagger} \geqslant E_i^{m,r*} - e_a^{m,r*} \geqslant E_j^{m,r*}$. Second, if $(i,j) = a \in \hat{L}(r)$, $E_j^{m,r\dagger} = \min\{E_i^{m,r\dagger} - e_a^{m,r*} + y_a\tau_a^{m,r*}\varepsilon,\ E_{max}^m b_{up}^m\}$; if $E_j^{m,r\dagger} = E_{max}^m b_{up}^m$, from constraint (5) we have $E_j^{m,r\dagger} = E_{max}^m b_{up}^m \geqslant E_j^{m,r*}$; if $E_j^{m,r\dagger} = E_i^{m,r\dagger} - e_a^{m,r*} + y_a\tau_a^{m,r*}\varepsilon$, then $E_j^{m,r\dagger} \geqslant E_i^{m,r*} - e_a^{m,r*} + y_a\tau_a^{m,r*}\varepsilon$, from constraints (7) and (19) we have $E_j^{m,r\dagger} \geqslant E_i^{m,r*} - e_a^{m,r*} + y_a\hat{\tau}_a^{m,r*}\varepsilon \geqslant E_j^{m,r*}$. Therefore, based on $E_{O(w)}^{m,r\dagger} = E_0^m \geqslant E_{O(w)}^{m,r*}$, we will always have $E_i^{m,r\dagger} \geqslant E_i^{m,r*},\ \forall\ i \in N(r)$. Moreover, from constraint (6) we have $E_i^{m,r\dagger} \geqslant E_i^{m,r*} \geqslant E_{max}^m b_{lo}^m,\ \forall\ i \in N(r)$.

(d) We prove that $\hat{\tau}_a^{m,r\dagger}$ and $\tau_a^{m,r*}$ satisfies constraints (7) and (12), i.e., $\hat{\tau}_a^{m,r\dagger} - \tau_a^{m,r*} \leqslant 0$ and $\hat{\tau}_a^{m,r\dagger} \geqslant 0,\ \forall\ a \in \hat{L}(r)$. First, if $E_j^{m,r\dagger} = E_i^{m,r\dagger} - e_a^{m,r*} + y_a\tau_a^{m,r*}\varepsilon$, then $\hat{\tau}_a^{m,r\dagger} = \frac{E_j^{m,r\dagger} - E_i^{m,r\dagger} + e_a^{m,r*}}{y_a\varepsilon} = \tau_a^{m,r*}$, from constraint (13) we further have $\hat{\tau}_a^{m,r\dagger} \geqslant 0$. Second, if $E_j^{m,r\dagger} = E_{max}^m b_{up}^m$, we must have $E_i^{m,r\dagger} - e_a^{m,r*} + y_a\tau_a^{m,r*}\varepsilon \geqslant E_{max}^m b_{up}^m$ because $E_j^{m,r\dagger} = \min\{E_i^{m,r\dagger} - e_a^{m,r*} + y_a\tau_a^{m,r*}\varepsilon,\ E_{max}^m b_{up}^m\}$, then $\hat{\tau}_a^{m,r\dagger} = \frac{E_j^{m,r\dagger} - E_i^{m,r\dagger} + e_a^{m,r*}}{y_a\varepsilon} = \frac{E_{max}^m b_{up}^m - E_i^{m,r\dagger} + e_a^{m,r*}}{y_a\varepsilon} \leqslant \tau_a^{m,r*}$, moreover because we have proved that $E_i^{m,r\dagger} \leqslant E_{max}^m b_{up}^m,\ \forall\ i \in N(r)$, $\hat{\tau}_a^{m,r\dagger} = \frac{E_{max}^m b_{up}^m - E_i^{m,r\dagger} + e_a^{m,r*}}{y_a\varepsilon} \geqslant 0$.

Based on the above discussions, we can see that $e_a^{m,r*}$, $d_a^{m,r*}$, $\tau_a^{m,r*}$, $\hat{\tau}_a^{m,r\dagger}$ and $E_i^{m,r\dagger}$ is a feasible solution of P1.

Appendix C. The solution procedure of BC/WC-MMUE

For the convenience of readers, below we repeat the formulations of BC/WC-MMUE.

BC/WC-MMUE:

$$\min/\max_{(\boldsymbol{\beta},\boldsymbol{\chi},\boldsymbol{\lambda},\boldsymbol{\mu},\boldsymbol{\xi},\boldsymbol{\psi},\boldsymbol{\omega},\boldsymbol{\alpha},\boldsymbol{f},\boldsymbol{h},\boldsymbol{v},\boldsymbol{\pi},\boldsymbol{e},\boldsymbol{d},\boldsymbol{\tau},\hat{\boldsymbol{\tau}},\boldsymbol{E})} \quad \Omega_1 \times TSTC + \Omega_2 \times TFC + \Omega_3 \times TEC$$

s.t. MMUE conditions (5)-(64), definitional constraints (89)-(93).

Since it is straightforward to convert a maximization problem into a minimization problem, we only show the solution procedure for the minimization scenario, i.e., the BC-MMUE. First, all complementarity constraints in the problem can be given by the following generalized form:

$$0 \leq F_{ind}(\boldsymbol{x_{ind}}) \perp x_{ind} \geq 0$$

where $\perp$ is the orthogonal sign representing the inner product of two vectors is zero, x_{ind} is a variable with index *ind* and $F_{ind}(\boldsymbol{x_{ind}})$ is a function of vector $\boldsymbol{x_{ind}}$. To illustrate, for constraints $0 \leq \left(\sum_{a\in A(r)} c_a^{m,r} - \pi_m^w\right) \perp f_r^m \geq 0,\ \ x_{ind} = f_r^m,\ \ ind = r \in R_m^w$, and $F_{ind}(\boldsymbol{x_{ind}}) = \sum_{a\in A(r)} c_a^{m,r} - \pi_m^w$. For each group of complementarity constraints, we define two index sets Λ_x and $\overline{\Lambda}_x$ to respectively track

the component of single variable x and formula $F(x)$ required to be zero:

$$\Lambda_x^k = \{ind: x_{ind} = 0\},$$

$$\overline{\Lambda}_x^k = \{ind: F_{ind}(\boldsymbol{x_{ind}}) = 0\}$$

Note that, here superscript k indicates the iteration of the solution procedure, which will be introduced below. Based on Λ_x and $\overline{\Lambda}_x$, a restricted version of BC-MMUE, denoted as R-BC-MMUE, can be formulated as the following nonlinear programs:

R-BC-MMUE:

$$\min_{(\boldsymbol{\beta},\boldsymbol{\chi},\boldsymbol{\lambda},\boldsymbol{\mu},\boldsymbol{\xi},\boldsymbol{\eta},\boldsymbol{\zeta},\boldsymbol{\psi},\boldsymbol{\omega},\boldsymbol{\alpha},\boldsymbol{f},\boldsymbol{h},\boldsymbol{v},\boldsymbol{\pi},\boldsymbol{e},\boldsymbol{d},\boldsymbol{\tau},\hat{\boldsymbol{\tau}},\boldsymbol{E})} \Omega_1 \times TSTC + \Omega_2 \times TFC + \Omega_3 \times TEC$$

s.t. (56)-(61) and

$$x_{ind} = 0 \quad \forall\, ind \in \Lambda_x^k$$

$$F_{ind}(\boldsymbol{x_{ind}}) = 0 \quad \forall\, ind \in \overline{\Lambda}_x^k$$

$$x_{ind} \geq 0 \quad \forall\, ind \notin \Lambda_x^k$$

$$F_{ind}(\boldsymbol{x_{ind}}) \geq 0 \quad \forall\, ind \notin \overline{\Lambda}_x^k$$

where $\boldsymbol{x_{ind}} = (\boldsymbol{\beta}, \boldsymbol{\chi}, \boldsymbol{\lambda}, \boldsymbol{\mu}, \boldsymbol{\xi}, \boldsymbol{\eta}, \boldsymbol{\zeta}, \boldsymbol{\psi}, \boldsymbol{\omega}, \boldsymbol{\alpha}, \boldsymbol{f}, \boldsymbol{h}, \boldsymbol{v}, \boldsymbol{\pi}, \boldsymbol{e}, \boldsymbol{d}, \boldsymbol{\tau}, \hat{\boldsymbol{\tau}}, \boldsymbol{E})$; the right part of $F_{ind}(\boldsymbol{x_{ind}}) \perp x_{ind}$, i.e., x_{ind}, can be $\beta_a^{m,r}$, $\chi_{ij}^{m,r}$, $\lambda_a^{m,r}$, $\mu_a^{m,r}$, $\xi_a^{m,r}$, $\eta_a^{m,r}$, $\zeta_a^{m,r}$, $\psi_i^{m,r}$, $\omega_i^{m,r}$, $\alpha_{O(w)}^{m,r}$, f_r^m, $e_a^{m,r}$, $d_a^{m,r}$, $\tau_a^{m,r}$, $\hat{\tau}_a^{m,r}$, $E_i^{m,r}$ and each of them has a corresponding $F_{ind}(\boldsymbol{x_{ind}})$.

At last, the iterative procedure of solving BC-MMUE is as follows:

Step 0: Solve the problem MMUE-NLP, and obtain the solution of vector $(\boldsymbol{\beta}, \boldsymbol{\chi}, \boldsymbol{\lambda}, \boldsymbol{\mu}, \boldsymbol{\xi}, \boldsymbol{\eta}, \boldsymbol{\zeta}, \boldsymbol{\psi}, \boldsymbol{\omega}, \boldsymbol{\alpha}, \boldsymbol{f}, \boldsymbol{h}, \boldsymbol{v}, \boldsymbol{\pi}, \boldsymbol{e}, \boldsymbol{d}, \boldsymbol{\tau}, \hat{\boldsymbol{\tau}}, \boldsymbol{E})$. Based on the solution, set $k = 1$ and initialize all index sets Λ_x^k and $\overline{\Lambda}_x^k$.

Step 1: Let $(\boldsymbol{\beta}, \boldsymbol{\chi}, \boldsymbol{\lambda}, \boldsymbol{\mu}, \boldsymbol{\xi}, \boldsymbol{\eta}, \boldsymbol{\zeta}, \boldsymbol{\psi}, \boldsymbol{\omega}, \boldsymbol{\alpha}, \boldsymbol{f}, \boldsymbol{h}, \boldsymbol{v}, \boldsymbol{\pi}, \boldsymbol{e}, \boldsymbol{d}, \boldsymbol{\tau}, \hat{\boldsymbol{\tau}}, \boldsymbol{E})^k$ solve R-BC-MMUE, and obtain the multipliers associated with constraints $x_{ind} = 0$, denoted as γ_{ind}^x.

Step 2: Update index sets defined as follows:

$$\Gamma^{x,k} = \{ind \in \Lambda_x^k \cap \overline{\Lambda}_x^k: \gamma_{ind}^x < 0\}$$

If all these index sets are empty, stop and $(\boldsymbol{\beta}, \boldsymbol{\chi}, \boldsymbol{\lambda}, \boldsymbol{\mu}, \boldsymbol{\xi}, \boldsymbol{\eta}, \boldsymbol{\zeta}, \boldsymbol{\psi}, \boldsymbol{\omega}, \boldsymbol{\alpha}, \boldsymbol{f}, \boldsymbol{h}, \boldsymbol{v}, \boldsymbol{\pi}, \boldsymbol{e}, \boldsymbol{d}, \boldsymbol{\tau}, \hat{\boldsymbol{\tau}}, \boldsymbol{E})^k$ is strongly stationary. Otherwise, do the following and go to Step 1:

(a) Set

$$\Lambda_x^{k+1} = \Lambda_x^k - \Gamma^{x,k}$$

(b) Set

$$\overline{\Lambda}_x^{k+1} = \{ind: F_{ind}(\boldsymbol{x_{ind}}) = 0\}$$

(c) Set $k = k + 1$

It should be noted that, because MMUE-NLP is solved using a column generation algorithm, the number of generated routes for some O-D pairs may be very small and thus limit the search space of the above algorithm. To deal with this issue, after solving MMUE-NLP and obtaining a limited route set, we can generate a number of additional unutilized routes to supplement the route set and solve the MMUE-NLP again over the new route set.

References

Aghassi, M., Bertsimas, D., Perakis, G., 2006. Solving asymmetric variational inequalities via convex optimization. Oper. Res. Lett. 34 (5), 481–490.

Ayala, R., 2014. The Value of Travel Time Savings: Departmental Guidance for Conducting Economic Evaluations Revision 2. Office of the Secretary of Transportation, US Department of Transportation, Washington DC.

Alternative Fuels Data Center, 2014. Fuel Properties Comparison. United States Department of Energy. https://www.afdc.energy.gov/fuels/fuel_comparison_chart.pdf (accessed August 28, 2017).

Alternative Fuels Data Center, 2017. Fuel Prices. United States Department of Energy. https://www.afdc.energy.gov/fuels/prices.html (accessed August 28, 2017).

American Trucking Association, 2016a. ATA American Trucking Trends 2016.

American Trucking Association, 2016b. U.S. Freight Transportation Forecast to 2027.

Ben-Tal, A., Nemirovski, A., 2002. Robust optimization–methodology and applications. Math. Program. 92 (3), 453–480.

Bell, M.G.H., Iida, Y., 1997. Transportation Network Analysis. John Wiley and Sons, West Sussex, England.

Boyce, D.E., 1984. Urban transportation network-equilibrium and design models: recent achievements and future prospects. Environ. Plann. A 16 (11), 1445–1474.

Boys, J.T., Covic, G.A., Elliott, G.A.J., 2002. Pick-up transformer for ICPT applications. Electron. Lett. 38 (21), 1276–1278.

Burton, J., Walkowicz, K., Sindler, P., Duran, A., 2013. In-use and vehicle dynamometer evaluation and comparison of class 7 hybrid electric and conventional diesel delivery trucks. SAE Int. J. Commer. Veh. 6 (2013–01-2468), 545–554.

California Electric Transportation Coalition (CalETC), 2015. Heavy-Duty Alternative Fuel Trucks.

Chen, L., Nagendra, G.R., Boys, J.T., Covic, G.A., 2015. Double-coupled systems for IPT roadway applications. IEEE J. Emerging Selected Top. Power Electron. 3 (1), 37–49.

Chen, Z., He, F., Yin, Y., 2016. Optimal deployment of charging lanes for electric vehicles in transportation networks. Transport. Res. Part B: Methodol. 91, 344–365.

Chen, Z., Liu, W., Yin, Y., 2017. Deployment of stationary and dynamic charging infrastructure for electric vehicles along traffic corridors. Transport. Res. Part C: Emerging Technol. 77, 185–206.
Chen, Z., Yin, Y., Song, Z., 2018. A cost-competitiveness analysis of charging infrastructure for electric bus operations. Transport. Res. Part C: Emerging Technol. 93, 351–366.
Chinneck, J.W., 2006. Practical optimization: a gentle introduction. Systems and Computer Engineering), Carleton University, Ottawa. http://www.sce.carleton.ca/faculty/chinneck/po.html.
Choi, S., Huh, J., Lee, W.Y., Lee, S.W., Rim, C.T., 2013. New cross-segmented power supply rails for roadway-powered electric vehicles. IEEE Trans. Power Electron. 28 (12), 5832–5841.
Cirimele, V., Freschi, F., Guglielmi, P., 2014. Wireless power transfer structure design for electric vehicle in charge while driving. Electrical Machines (ICEM), 2014 International Conference on 2461–2467.
Covic, G.A., Elliott, G., Stielau, O.H., Green, R.M., Boys, J.T., 2000. The design of a contact-less energy transfer system for a people mover system. Power System Technology, 2000. Proceedings. PowerCon 2000International Conference on. 1, 79–84.
Deflorio, F., Castello, L., 2017. Dynamic charging-while-driving systems for freight delivery services with electric vehicles: Traffic and energy modelling. Transport. Res. Part C: Emerging Technol. 81, 342–362.
Davis, S.C., Diegel, S.W., Boundy, R.G., 2016. Transportation Energy Data Book: Edition 35. Department of Energy, Oak Ridge, Tennessee.
de Andrade, G.R., Chen, Z., Elefteriadou, L., Yin, Y., 2017. Multiclass traffic assignment problem with flow-dependent passenger car equivalent value of trucks. Transport. Res. Rec.: J. Transport. Res. Board 2667, 131–141.
Dijkstra, E.W., 1959. A note on two problems in connexion with graphs. Numerische mathematik 1 (1), 269–271.
Dreher, D.B., Harley, R.A., 1998. A fuel-based inventory for heavy-duty diesel truck emissions. J. Air Waste Manag. Assoc. 48 (4), 352–358.
Drud, A.S., 1994. CONOPT—a large-scale GRG code. ORSA J. Comput. 6 (2), 207–216.
Farahani, R.Z., Miandoabchi, E., Szeto, W.Y., Rashidi, H., 2013. A review of urban transportation network design problems. Eur. J. Oper. Res. 229 (2), 281–302.
Farvaresh, H., Sepehri, M.M., 2011. A single-level mixed integer linear formulation for a bi-level discrete network design problem. Transport. Res. Part E: Log. Transport. Rev. 47 (5), 623–640.
Fletcher, R., Leyffer, S., 2004. Solving mathematical programs with complementarity constraints as nonlinear programs. Optimization Methods Software 19 (1), 15–40.
Friesz, T.L., 1985. Transportation network equilibrium, design and aggregation: key developments and research opportunities. Transport. Res. Part A: General 19 (5–6), 413–427.
Fuller, M., 2016. Wireless charging in California: range, recharge, and vehicle electrification. Transport. Res. Part C: Emerging Technol. 67, 343–356.
Gao, Z., Lin, Z., Franzese, O., 2017. Energy consumption and cost savings of truck electrification for heavy-duty vehicle applications. Transport. Res. Rec.: J. Transport. Res. Board 2628, 99–109.
Grünjes, H.G., Birkner, M., 2012. Electro mobility for heavy duty vehicles (HDV): The Siemens eHighway System. In: 12th International Symposium on Heavy Vehicle Transportation Technology, Stockholm, Sweden.
Guo, X., Yang, H., 2010. Pareto-improving congestion pricing and revenue refunding with multiple user classes. Transport. Res. Part B: Methodol. 44 (8), 972–982.
He, F., Yin, Y., Lawphongpanich, S., 2014. Network equilibrium models with battery electric vehicles. Transport. Res. Part B: Methodol. 67, 306–319.
He, F., Yin, Y., Zhou, J., 2015. Deploying public charging stations for electric vehicles on urban road networks. Transport. Res. Part C: Emerging Technol. 60, 227–240.
He, F., Yin, Y., Wang, J., Yang, Y., 2016. Sustainability SI: optimal prices of electricity at public charging stations for plug-in electric vehicles. Networks Spatial Econ. 16 (1), 131–154.
He, Yi, Song, Ziqi, Zhang, Lihui, 2018. Time-dependent transportation network design considering construction impact. J. Adv. Transport. 2018, 2738930. https://doi.org/10.1155/2018/2738930. 18 pp.
Huh, J., Lee, S.W., Lee, W.Y., Cho, G.H., Rim, C.T., 2011. Narrow-width inductive power transfer system for online electrical vehicles. IEEE Trans. Power Electron. 26 (12), 3666–3679.
Huang, C.Y., Boys, J.T., Covic, G.A., Budhia, M., 2009. Practical considerations for designing IPT system for EV battery charging. 2009 IEEE Vehicle Power and Propulsion Conference 402–407.
Jang, Y.J., Jeong, S., Ko, Y.D., 2015. System optimization of the on-line electric vehicle operating in a closed environment. Comput. Ind. Eng. 80, 222–235.
Jiang, N., Xie, C., Waller, S., 2012. Path-constrained traffic assignment: model and algorithm. Transport. Res. Rec.: J. Transport. Res. Board 2283, 25–33.
Jiang, N., Xie, C., Duthie, J.C., Waller, S.T., 2014. A network equilibrium analysis on destination, route and parking choices with mixed gasoline and electric vehicular flows. EURO J. Transport. Log. 3 (1), 55–92.
Jiang, N., Xie, C., 2014. Computing and analyzing mixed equilibrium network flows with gasoline and electric vehicles. Comput.-Aided Civ. Infrastruct. Eng. 29 (8), 626–641.
Johannesson, L., Murgovski, N., Jonasson, E., Hellgren, J., Egardt, B., 2015. Predictive energy management of hybrid long-haul trucks. Control Eng. Pract. 41, 83–97.
Lawphongpanich, S., Hearn, D.W., 2004. An MPEC approach to second-best toll pricing. Math. Program. 101 (1), 33–55.
Lawphongpanich, S., Yin, Y., 2010. Solving the Pareto-improving toll problem via manifold suboptimization. Transport. Res. Part C: Emerging Technol. 18 (2), 234–246.
Leventhal, T., Nemhauser, G., Trotter Jr., L., 1973. A column generation algorithm for optimal traffic assignment. Transport. Sci. 7 (2), 168–176.
Liang, C., Fan, B.Q., Cheng, J.Q., 2011. Multi-class network equilibrium based on the variable PCE of mixed traffic. J. Transport. Syst. Eng. Inf. Technol. 3, 014.
Liang, C., Fan, B.Q., Dong, J.S., He, Y.H., 2013. A network equilibrium model with variable PCE and its applications. J. Syst. Manage. 6, 021.
Limb, B.J., Crabb, B., Zane, R., Bradley, T.H., Quinn, J.C., 2016. Economic feasibility and infrastructure optimization of in-motion charging of electric vehicles using wireless power transfer. In: Emerging Technologies: Wireless Power Transfer (WoW), 2016 IEEE PELS Workshop on, pp. 42–46.
Liu, Z., Song, Z., 2017. Robust planning of dynamic wireless charging infrastructure for battery electric buses. Transport. Res. Part C: Emerging Technol. 83, 77–103.
Liu, Z., Song, Z., He, Y., 2017. Optimal deployment of dynamic wireless charging facilities for an electric bus system. Transport. Res. Rec.: J. Transport. Res Board 2647, 100–108.
Liu, Z., Song, Z., 2018. Network user equilibrium of battery electric vehicles considering flow-dependent electricity consumption. Transport. Res. Part C: Emerging Technol. 95, 516–544.
Lou, Y., Yin, Y., Lawphongpanich, S., 2010. Robust congestion pricing under boundedly rational user equilibrium. Transport. Res. Part B: Methodol. 44 (1), 15–28.
Luo, Z.Q., Pang, J.S., Ralph, D., 1996. Mathematical Programs with Equilibrium Constraints. Cambridge University Press.
Matthews, H.S., 1999. The external costs of air pollution and the environmental impact of the consumer in the US economy. Unpublished Ph. D. dissertation. Graduate School of Industrial Administration: Pittsburgh, PA.
Morris, C., 2015. Utah State University builds a dynamic wireless charging test track (2015) http://chargedevs.com/features/utah-state-university-builds-a-dynamic-wireless-charging-test-track/ (accessed December 05, 2016).
Nguyen, S., Dupuis, C., 1984. An efficient method for computing traffic equilibria in networks with asymmetric transportation costs. Transport. Sci. 18 (2), 185–202.
Nagurney, A., 2000. A multiclass, multicriteria traffic network equilibrium model. Math. Comput. Modell. 32 (3–4), 393–411.
Okui, N., 2016. A study on improvement of fuel economy of heavy duty hybrid trucks with new type of hybrid electric assist engine system. SAE Int. J. Commer. Veh. 9 (2016–01-2358), 41–50.
PATH team, 1996. Roadway Powered Electric Vehicle Project Parametric Studies: Phase 3D Final Report. California Partners for Advanced Transit and Highways Research Report.
Polak, E., Royset, J.O., 2005. On the use of augmented Lagrangians in the solution of generalized semi-infinite min-max problems. Comput. Optimization Appl. 31 (2), 173–192.
Riemann, R., Wang, D.Z., Busch, F., 2015. Optimal location of wireless charging facilities for electric vehicles: flow-capturing location model with stochastic user equilibrium. Transport. Res. Part C: Emerging Technol. 58, 1–12.

Rosenthal, R.E., 2012. GAMS – A User's Guide. GAMS Development Corporation, Washington, DC.
Szeto, W.Y., Jaber, X., Wong, S.C., 2012. Road network equilibrium approaches to environmental sustainability. Transport Rev. 32 (4), 491–518.
Scania, 2016. World's first electric road opens in Sweden https://www.scania.com/group/en/worlds-first-electric-road-opens-in-sweden/ (accessed December 05, 2016).
Sheffi, Y., 1985. Urban Transportation Network. Pretince Hall.
Siemens, 2015. Siemens To Bring eHighway Demonstration To California http://siemensusa.synapticdigital.com/US/siemens-to-bring-ehighway-demonstration-to-california/s/65152173-d3a5-459d-b0fd-19a73ee01c6b (accessed December 05, 2016).
Song, Z., Yin, Y., Lawphongpanich, S., 2009. Nonnegative Pareto-improving tolls with multiclass network equilibria. Transport. Res. Rec.: J. Transport. Res. Board 2091, 70–78.
Song, Z., Yin, Y., Lawphongpanich, S., Yang, H., 2014. A Pareto-improving hybrid policy for transportation networks. J. Adv. Transport. 48 (3), 272–286.
Song, Z., He, Y., Zhang, L., 2017. Integrated planning of park-and-ride facilities and transit service. Transport. Res. Part C: Emerging Technol. 74, 182–195.
Sripad, S., Viswanathan, V., 2017. Performance metrics required of next-generation batteries to make a practical electric semi truck. ACS Energy Lett. 2 (7), 1669–1673.
Still, G., 1999. Generalized semi-infinite programming: theory and methods. Eur. J. Oper. Res. 119 (2), 301–313.
Suh, N.P., Cho, D.H., Rim, C.T., 2011. Design of on-line electric vehicle (OLEV). In: Global Product Development. Springer, Berlin Heidelberg, pp. 3–8.
Torrey, W.F., Murray, D., 2016. An Analysis of the Operational Costs of Trucking: 2016 Update. Arlington, Virginia.
Transportation Research Board (TRB), 2010. Highway Capacity Manual 2010. Washington, D.C.
US Department of Energy (USDOE), 2017a. https://www.fueleconomy.gov/feg/evtech.shtml (accessed August 29, 2017).
US Department of Energy (USDOE), 2017b. http://www.fueleconomy.gov/feg/atv.shtml (accessed August 29, 2017).
Wang, D.Z., Liu, H., Szeto, W.Y., 2015. A novel discrete network design problem formulation and its global optimization solution algorithm. Transport. Res. Part E: Log. Transport. Rev. 79, 213–230.
Wang, T.G., Xie, C., Xie, J., Waller, S.T., 2016. Path-constrained traffic assignment: a trip chain analysis under range anxiety. Transp. Res. Part C 68, 447–461.
Xie, C., Jiang, N., 2016. Relay requirement and traffic assignment of electric vehicles. Comput.-Aided Civ. Infrastruct. Eng. 31 (8), 580–598.
Xie, C., Wang, T.G., Pu, X., Karoonsoontawong, A., 2017. Path-constrained traffic assignment: modeling and computing network impacts of stochastic range anxiety. Transp. Res. Part B 103, 136–157.
Xu, X., Chen, A., Yang, C., 2016. A review of sustainable network design for road networks. KSCE J. Civ. Eng. 20 (3), 1084–1098.
Xu, M., Meng, Q., Liu, K., 2017. Network user equilibrium problems for the mixed battery electric vehicles and gasoline vehicles subject to battery swapping stations and road grade constraints. Transport. Res. Part B: Methodol. 99, 138–166.
Yang, H.H., Bell, M.G., 1998. Models and algorithms for road network design: a review and some new developments. Transport Rev. 18 (3), 257–278.
Yang, H., Ye, H., Li, X., Zhao, B., 2015. Speed limits, speed selection and network equilibrium. Transport. Res. Part C: Emerging Technol. 51, 260–273.
Yamada, T., Febri, Z., 2015. Freight transport network design using particle swarm optimisation in supply chain–transport supernetwork equilibrium. Transport. Res. Part E: Log. Transport. Rev. 75, 164–187.
Yin, Y., Yang, H., 2004. Optimal tolls with a multiclass, bicriteria traffic network equilibrium. Transp. Res. Rec. 1882, 45–52.
Zheng, H., He, X., Li, Y., Peeta, S., 2017. Traffic equilibrium and charging facility locations for electric vehicles. Networks Spatial Econ. 17 (2), 435–457.